Comparative study of molecular dynamics and phase field modelling for brittle fracture.

Dissertation for the fulfillment of

Masters of technology

by

Utkarsh Rawat

CENTER FOR NANOTECHNOLOGY
INDIAN INSTITUTE OF TECHNOLOGY ROORKEE
ROORKEE - 247 667 (INDIA)
MAY, 2019

©INDIAN INSTITUTE OF TECHNOLOGY ROORKEE, ROORKEE-2019
ALL RIGHTS RESERVED

INDIAN INSTITUTE OF TECHNOLOGY ROORKEE
ROORKEE

CANDIDATE'S DECLARATION

I hereby certify that the work which is being presented in the seminar report entitled **"Comparative study of molecular dynamics and phase field modeling for brittle fracture."** in partial fulfillment of the requirements for the award of the Degree of Masters of technology and submitted in the Center for nanotechnology of the Indian institute of technology Roorkee, Roorkee is an authentic record of my own work carried out during the period from June 2018 to May 2019 under the supervision of Dr. Rajib Chowdhury, Associate Professor, Department of Civil engineering, Indian institute of technology Roorkee, Roorkee.

The matter presented in this thesis has not been submitted by me for the award of any other degree of this or any other Institute.

(Utkarsh Rawat)

This is to certify that the above statement made by the candidate is correct to the best of my knowledge.

(Dr. Rajib Chowdhury)
Supervisor

Date:

भारतीय प्रौद्योगिकी संस्थान रुड़की
INDIAN INSTITUTE OF TECHNOLOGY ROORKEE

Abstract

Center of nanotechnology

Master of technology

Comparative study of molecular dynamics and phase field modeling

by Utkarsh Rawat

In this study, molecular dynamics fracture simulation of a brittle single layer graphene sheet is performed to give us the parameters needed to perform phase field fracture modeling. Molecular dynamics simulation encompasses the physical nature of the fracture and is discrete while phase field is a continuum phenomenological method of performing these simulations. By deriving parameters for phase field simulation through atomistic simulation an attempt has been made to establish a link between different scale models and to establish a correspondence in predicting crack path. Using the parameters obtained through molecular dynamics accurate path prediction and branching of cracks were observed through phase field modeling when compared to physics-based molecular dynamics. The force at which fracture occurred was found to be comparable, despite stiffness showing some difference between two models. The relation between the two models can be established where the continuum model retains the essence of atomic details. This would open up a path for multiscale simulations which are much more accurate and reliable.

भारतीय प्रौद्योगिकी संस्थान रुड़की
INDIAN INSTITUTE OF TECHNOLOGY ROORKEE

Acknowledgements

I would like to express my gratitude to my guide Dr. Rajib Chowdhury, Associate Professor for his guidance. His feedback was essential in completing this thesis work. I am also grateful to my family and friends for their support and encouragement.

Date: (Utkarsh Rawat)

भारतीय प्रौद्योगिकी संस्थान रुड़की
INDIAN INSTITUTE OF TECHNOLOGY ROORKEE

Contents

Abstract v

Acknowledgements vii

1 Introduction 1
1.1 General 1
1.2 Objective of the study 2
1.3 Organization of report 2

2 Literature Review 3
2.1 General 3
2.2 Literature study 3

3 Fracture mechanics and numerical techniques 7
3.1 Introduction 7
3.2 Linear Elastic Fracture Mechanics 7
3.2.1 Griffith's criterion 8
3.2.2 Variational formulation of brittle fracture 10
3.3 Numerical Technique 11
3.3.1 Basics of numerical technique 11
3.3.2 Finite Difference Method 12
3.3.3 Finite Element Method 13
Elements and nodes 13
Isoparametric Representation 14
Shape Functions 15
Chain rule and Jacobian 17

4 Phase Field Modeling 19
4.1 Introduction 19

4.2 Cahn Hilliard Equation 19
4.3 Phase Field Derivation 20
4.3.1 Finite Element Implementation 21
4.4 Phase Field Model for fracture modeling 24
4.5 Phase Field Fracture FEM model 26
Barrier term 29

5 Molecular Dynamics 31
5.1 Introduction 31
5.2 Interatomic Interaction 31
5.3 Integration algorithm 33
The Varlet Algorithm 34
The Velocity Varlet Algorithm 35
5.4 Statistical mechanics 35
5.5 Ensemble 36
5.6 Perodic Boundary Conditions 36
5.7 Molecular Dynamics simulation algorithm 36

6 Simulation 39
6.1 General 39
6.2 Molecular Dynamics 39
6.3 Phase field simulation 41

7 Results and Discussion 45
7.1 General 45
7.2 Molecular Dynamics 45
Simulation results 45
7.3 Phase Field Modeling 48
7.4 Discussion 51

8 Conclusion and future prospects 55
8.1 Conclusion 55
8.2 Future work 56

Bibliography 57

List of Figures

3.1 Modes Of Fracture . . . 8
3.2 An arbitrary cracked body . . . 9
3.3 Five point stencil used in space discretisation . . . 13
3.4 Figure representing nodes (blue circles) and elements (blue horizontal lines) 14
3.5 1) Three node 2) Four node 3) Eight node Isoparametric representation of an element . . . 15
3.6 Simple linear shape functions . . . 16
3.7 Process of formation of global stiffness matrix from element stiffness matrix 18

4.1 Spinodal decomposition of binary alloy . . . 20
4.2 Double well potential . . . 22
4.3 Figure representing the effect of length scale of the diffusive nature of the crack topology . . . 26

5.1 Interatomic potential vs interatomic distance . . . 32
5.2 Figure representing periodic boundary with main simulation cell in centre and its image surrounding it. When an atom leaves the periodic boundary its image enters the simulation cell from other side. . . . 37
5.3 Molecular dynamics algorithm . . . 38

6.1 Graphene structure . . . 40
6.2 Graphene sheet . . . 41
6.3 Stabilization of potential energy . . . 42
6.4 Stabilization of temperature . . . 42
6.6 20nm graphene sheet . . . 43
6.7 Finite element mesh . . . 44

7.1 Folds appear on the graphene sheet under strain . . . 47
7.2 Snapshots of SLGS undergoing fracture at different time-steps . . . 48
7.3 Stress concentration near the crack . . . 49

7.4 Stress-strain curve of graphene sheet 49
7.5 Load-displacement graph of phase field model 51
7.6 Snapshots phase field model undergoing fracture at different time-steps . . 52
7.7 Similarity between the crack branching prediction between MD and PFM . 53
7.8 Combined load-displacement graphs of MD and PF models. 54

List of Abbreviations

FEM	Finite Element Method
LEFM	Linear Elastic Fracture Mechanics
PFM	Phase Field Modeling
MD	Molecular Dynamics
PDE	Partial Diffirential Equation
FDM	Finite Difference Method
AIREBO	Adaptive Intermolecular Reactive Empirical Bond Order
SLGS	Single Layer Grephene Sheet
LAMMPS	Large-scale Atomic/Molecular Massively Parallel Simulator
CIF	Crystallographic Information File

भारतीय प्रौद्योगिकी संस्थान रुड़की
INDIAN INSTITUTE OF TECHNOLOGY ROORKEE

List of Symbols

Φ_{s}	Fracture surface energy
G_c	Critical energy release rate
Γ	Crack or discontinuity
Φ_{int}	Total internal energy
Φ_e	elastic energy
ψ	Elastic energy density
ϕ	Scalar field variable
E	Youngs constant
ν	Poissons ratio
σ	Stress

भारतीय प्रौद्योगिकी संस्थान रुड़की
INDIAN INSTITUTE OF TECHNOLOGY ROORKEE

Chapter 1

Introduction

1.1 General

Crack imitation and prediction has been gaining traction in term of research in recent years. One of the main goals of studying fracture mechanics is to be able to improve our understanding of its underlying process at the atomic scale and to be able to predict its consequences at the macroscale. Brittle fracture, in particular, has been given the spotlight as catastrophic failures occurring in the past have been very expansive. A brittle fracture occurs when atomic bonds are suddenly broken with a relatively small deformation of the specimen. The cause of sudden breakage is due to stress being shared by a small group of atoms, ie local strain energy exceeds the energy keeping the bonds together. A wide variety of methods and techniques has been used to study such failures. These methods can be classified based on the length and time scale they work most effectively on.

Molecular dynamics simulation have increasingly become an important tool to study various small scale phenomenon and give important insight which may be difficult to obtain through experiments. Times scale of these molecular dynamics ranges around picoseconds to microseconds, making them appropriate to study such high speed crack propagation as that in a brittle material. Valuable insights were obtained from these experiments on crack dynamics, however systematic analysis of mechanical properties at those scales and link between continuum approaches to study fracture behavior have still not been established.MD simulations while being efficient and accurate at molecular state are not practical at larger meso-scales.

This constrained nature of molecular dynamics can be handled by using continuum mechanical methods where the material is treated at a continuous system rather than a discrete system composed of atoms. One such approach is Phase-field modeling (PFM) which owing to its versatility,has distinguished itself as a new powerful tool for studying continuum mechanical problems. Phase field modeling is phenomenological in nature and also have a good accuracy and resource tradeoff.

1.2 Objective of the study

The objective of the study is to study brittle fracture in nanoscale using physics based molecular dynamics and phenomenological phase field modeling. Thereafter conclusions are to be made on the possibility of convergence of discrete and continuum approaches based on the equivalency of the results and the parameters involved. This would thereby help in the possibility of multiscale modeling.

1.3 Organization of report

1. Chapter 1 Introduction
2. Chapter 2 Literature Review
3. Chapter 3 Fracture mechanics and numerical techniques
4. Chapter 4 Phase Field Modeling
5. Chapter 5 Molecular Dynamics
6. chapter 6 Simulation
7. Chapter 7 Results and Discussion
8. Chapter 8 Conclusion and future prospects

Chapter 2

Literature Review

2.1 General

Griffith and Irwin in their pioneering works along with the variational formulations of crack propagation presented by Blaise Bourdin et. al[10] has been the basis of a well-defined and established framework on energy based brittle fracture. The work done by them has continued to be developed and added to. Some of these quasi-static brittle fracture models have been successfully been implemented in the works of Bourdin, Miehe [33], Verhoosel and Borst[42], Ambati[2], Kuhn[28] to name a few. To implement these variational formulations in robust finite element implantation, the phenomenological phase variable is incorporated. This variable replaces the sharp crack topology by a diffused interface. This idea of diffusive interface is physics based and was used by ohn W. Cahn and Hilliard[13] to describe a binary alloy system by a partial differential equation. Graphene has been seen as the next step in material science evolution. It's exceptional mechanical, thermal and electoral properties make it a very good candidate for the next-gen engineering products.

2.2 Literature study

Griffith and Irwin based on their thermodynamic framework for fracture propagation proposed that a crack begins propagation when the elastic strain energy at the crack tip is greater than or equal to the energy required to create two new crack surfaces. John W.

Cahn and Hilliard[10] work gave the Griffiths criterion a variational approach and improved upon Griffiths work by adding the ability to predict crack path. Phase field equation originates from Cahn-Hilliard equation derived from the work of [13]. It originated as a model to describe spinodal decomposition in a heterogeneous alloy. Two different partial differential equations, one conserved, by Cahn-Hilliard and non-conserved, by Allen and J. W. Cahn[1] was derived from this. These are the underlying equation of many other phase field model based on physics such as being used in image in painting Bertozzi[8], multiphase fluid flow Kim[26], phase separation Elliott and French[18], flow visualization Garcke et al[20] , the formation of quantum dots Garcke et al[20],pore migration in a temperature gradient L. Zhang et al[45] and tumour growth Cristini et al[16]. A regularised version of variational formulation of Griffiths formulation was proposed by Blaise Bourdin, Gilles A Francfort, et al[11] in which the sharp crack interface was approximated by a diffused interface, which can converge to sharp topology. From G. A. Francfort and J.-J. Marigo,[19]s work on variational formulation of Griffiths fracture models, a phase field model for quasi-static brittle fracture emerged. Their work was inspired by the works of B. Bourdin[9]. This formulation leads to an energy functional which closely relates to the potential presented by Mumford and Shah,[34] encountered in image segmentation. Ambrosio and Tortorelli[3] presented a phase field approximation of Mumford-shah potential which has its basis on the theory of convergence. According to Blaise Bourdin [10] this approximation facilitated the numerical solution the variational formulation produced by them. This model has recently been applied in a dynamics setting by Larsen[29] although no application for engineering structure was considered. An alternate formulation was presented by Miehe[33] for the quasi-static formulation in their recent works. This phase field approximation follows from continuum mechanics and has thermodynamic arguments. Miche et al.'s model is applicable to structures encountered in engineering application. Molecular dynamics simulation are becoming an important tool for investigating high speed crack propagation in materials. Molecular dynamic simulations have been used to study crack propagation Cindy L. Rountree et al[40] for inorganic materials such as Si_3N_4 Kalia et al.[24],SiO_2 C. L. Rountree et al,[39] and SiC Kikuchi et al[25].

Graphene owing to its exceptional mechanical and physical properties Kikuchi et al[25] Ando[5] is a promising candidate for the material to be used in next-generation nano-electronic and nano-composite materials. Graphene exhibits high thermal conductivity, specific surface area high charge carrier mobility and other important properties. It also has high hardness and elastic modulus. Fracture strength of graphene plays an important role in designing materials and structures. Omeltchenko et al[35] performed MD simulations using Tersoff-Benner potential for simulating crack propagation in a two million atom SLGS showing that crack path has a strong dependence on the initial crack orientation. Jin Jin Jin and Yuan[22] developed a method to calculate the J-integral and studies stationary cracks in graphene sheets. To validate the application of Griffith criterion for brittle fracture in graphene sheets Yin et al [44]performed series of MD simulations and concluded that fracture strength calculated from Griffith criterion remains equal to that of MD simulation until the crack size is more than 10nm. Below that difference can be as large as 15 percent. P. Zhang et al[46] performed fracture testing of single layer graphene sheets and polycrystalline graphene. They performed experimental and molecular dynamics simulation and found the results to be comparable. Le and Batra[30] on their testing of single edge crack found that j-integral depends upon crack length. They also noted that shorter cracks propagate faster than longer cracks but their propagation starts at a higher strain.

भारतीय प्रौद्योगिकी संस्थान रुड़की
INDIAN INSTITUTE OF TECHNOLOGY ROORKEE

Chapter 3

Fracture mechanics and numerical techniques

3.1 Introduction

In this chapter, fundamental concepts of linear elastic fracture mechanics are described briefly. Griffith's criteria and its variational formulation which forms the basis of its phase field model are also described. Also in this chapter numerical techniques are briefly covered which are used to solve the phase field fracture equation.

3.2 Linear Elastic Fracture Mechanics

Linear elastic fracture mechanics approaches fracture as a continuum problem without taking into account the atomistic details. Stress, strain and energy the only parameters describing the problem. The most important postulate of LEFM is that the material properties are linear throughout the domain.

In fracture mechanics, a crack can be characterized in one of the three primary modes and many secondary in combinations of those three.

1. MODE I-In this type of crack the force applied is perpendicular to the crack surface.
2. MODE II- In this type of crack the applied forces are parallel to the crack surface such that there is a sliding motion in the crack

3. MODE III- In this cracking mode the forces on the crack surfaces are parallel as well but the surfaces slide out of the plane to each other.

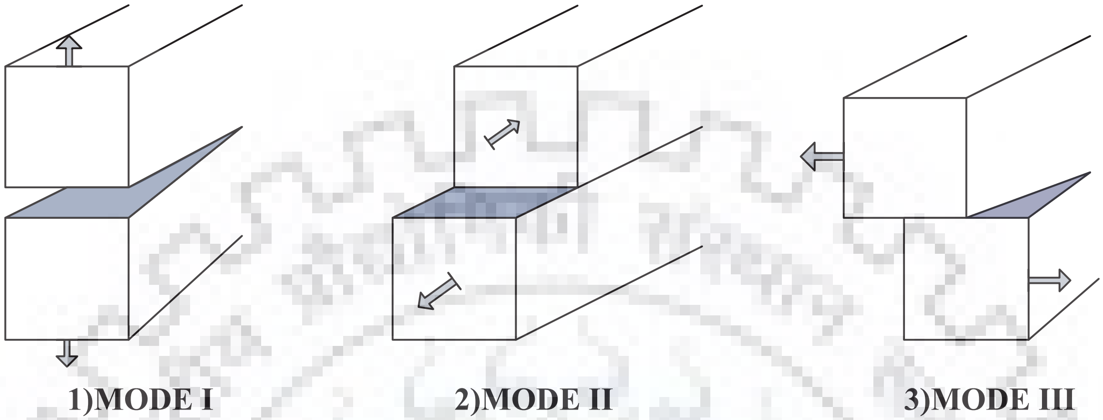

FIGURE 3.1: Modes Of Fracture

3.2.1 Griffith's criterion

During the 1920's Griffith analyzed crack growth in terms of energy.His postulates are considered as the first systematic study of fracture mechanics. He observed that fracture strength of materials is significantly less then what was theoretically suggested based on the bond strength calculations. His explanation was that this is due to the microscopic defects present in the material due to stress concentration.

In developing his theory, Griffith put forward an assumption that energy is dissipated in the creation of a new crack surface formed through crack Γ propagation. This energy is known as fracture energy Φ_s. This energy is equal to the surface area of the new area created through the crack formation with with proportionality constant depicted as critical strain energy release rate G_c

$$\Phi_s = \int_{\Gamma} \mathcal{G}_c d\Gamma \tag{3.1}$$

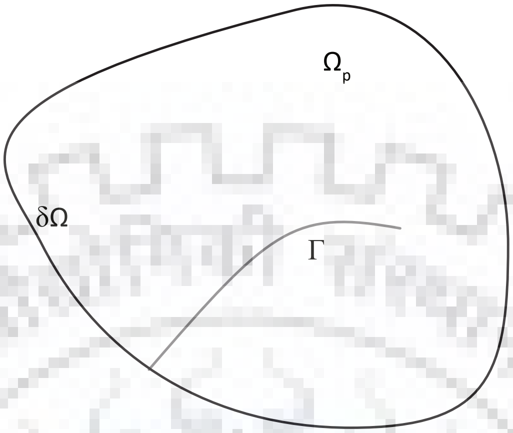

FIGURE 3.2: An arbitrary cracked body

Total internal energy Φ_{int} can, therefore, be written as the sun of fracture surface energy Φ_s required to form new surfaces and elastic energy Φ_e dissipated through the crack formation

$$\Phi_{int} = \Phi_e + \Phi_s \tag{3.2}$$

Work done is related to external energy as

$$\Phi_{ext} = -W_f \tag{3.3}$$

Under a constant displacement setting, it is assumed that work done is equal to zero. Also, if the displacement is performed in a quasi-static way, kinetic energy is neglected and is equal to zero. According to Griffith, in accordance with energy minimization crack will only grow if the total energy of the system decreases following crack propagation per unit length da Which can be written as

$$\mathcal{G} = \left|\frac{\mathrm{d}\Phi_e}{\mathrm{d}a}\right| > \frac{\mathrm{d}\Phi_s}{\mathrm{d}a} = \mathcal{G}_c \tag{3.4}$$

where G_c is energy release rate criterion which is also change in strain energy per unit increase in crack length as per the equation. The above equation can then predict when the crack will initiate, however crack path, crack branching, kinking cannot be predicted.

3.2.2 Variational formulation of brittle fracture

Francfort and Margio proposed a variational formulation of brittle fracture to overcome the deficiencies of Griffith's criteria. The main shortcomings of Griffiths criteria were

1. It cannot predict the crack initiation
2. It cannot predict the crack path
3. The phenomenon of crack jumping along the crack path cannot be realized.

Francfort and Margio utilised minimization of energy as their primary tool in formulating the variational approach for crack propagation. One main component in this energy equation was surface energy defined by a discontinuity Γ as

$$\Phi_s(\Gamma) = \int_{\Gamma} \mathcal{G}_c d\mathcal{H}^{d-1}(\Gamma) \tag{3.5}$$

$\mathcal{H}^{d-1}$ here is Hausdrofff measure. The material behaviour was considered linear and the displacement loading condition was considered as a linear function of time $(\dot{u}t)$. Elastic energy, taking these assumptions into account is given by

$$\Phi_e(\Gamma, u) = \int_{\Omega_p} \psi(\epsilon(u)) d\Omega \tag{3.6}$$

where ψ is given as

$$\psi_e(\epsilon) = \frac{1}{2}\lambda(\mathrm{tr}(\epsilon))^2 + \mu\epsilon : \epsilon \tag{3.7}$$

is elastic energy density and is a strain dependent function. As the system under consideration is of quasi-static nature, kinetic energy contribution can be considered to be zero and neglected. Also, work done on the body under the displacement loading condition is zero. This implies that the total energy of the body can simply be taken as surface and elastic energy's sum given as

$$\Phi_t = \Phi_e + \Phi_s \tag{3.8}$$

For crack evolution and propagation, energy minimization conditions are taken into account for each quasistatic step and only those sets of displacements $(u(x,t))$ are allowed which also maintains an irreversibility condition wherein crack cannot revert back even if energy is favorable. This condition gives the variational formulation ability to predict stable cracks, which grows due to incremental changes in the discontinuity and unstable cracks which are unstable and releases energy rabidly. This way all types of crack behavior like crack branching and nucleation can be handled, which is not possible with Griffiths theory.

3.3 Numerical Technique

Most of the modern fundamental theories of physics and engineering are expressed as a system of partial differential equations PDEs. Each PDE has its unique characteristics expressing the underlying phenomenon. Due to this no real unified theory to solve these PDEs exist as such we rely upon numerical approaches to get approximate solutions.

3.3.1 Basics of numerical technique

Numerical techniques in general use discretization of space to solve PDEs. Let

$$\frac{\partial u}{\partial t} = \frac{\partial^2 u}{\partial x^2} \tag{3.9}$$

be a PDE,such that u is a vector function of length x , u(x) in a domain Ω. Let

$$Lu = f, x \in \Omega \tag{3.10}$$

with boundary condition

$$Bu = 0, x \in \partial\Omega \tag{3.11}$$

where B and L are linear operations. Generally for solving a PDE using numerical approach we are actually finding the most appropriate function that can represent the function u(x) in question by a sum of functions known as trail/basis functions $\Phi_n(x)$. This can be represented as:

$$\widetilde{u}(x) = \sum_{n=0}^{N} a_n \phi_n(x) \tag{3.12}$$

Here $\widetilde{u}(x)$ approximates the function $u(x)$ with an unknown coefficients to be determined. A Residue R(error) is introduced here which is the difference between the original function and the approximated function.

In order to achieve the most accurate solution possible residue is to be minimized. Two of the most commonly used techniques for solving PDEs studied here.

3.3.2 Finite Difference Method

Finite difference method one of the simpler method for solving PDEs numerically. It is easier to code and compute using distributed environments. But due to its simplicity, it can have a lower accuracy as well as we need to define complex boundary conditions. Let a continuous function u be defined on a 1-D grid having spacing h, then the differential equations are defined as

The backward difference:

$$(\Delta u)_i^- = \frac{u_i - u_{i-1}}{h} \tag{3.13}$$

The forward difference:

$$(\Delta u)_i^+ = \frac{u_{i+1} - u_i}{h} \tag{3.14}$$

The centered difference:

$$(\Delta u)_i^\pm = \frac{u_{i+1} - u_{i-1}}{h} \tag{3.15}$$

The centered second difference:

$$\left(\Delta^2 u\right)_i = \frac{u_{i+1} - 2u_i + u_{i-1}}{h^2} \tag{3.16}$$

The centered second difference can be used to approximate the Laplace operator commonly used in PDEs. For a 2-D grid with grid points (x_i, y_j), the Laplace operator becomes

$$\left(\nabla^2 u\right)_{i,j} = \left(\Delta_{xx}^2 u\right)_{i,j} + \left(\Delta_{yy}^2 u\right)_{i,j} \tag{3.17}$$

which is equal to

$$\left(\nabla^2 u\right)_{i,j} = \frac{u_{i+1,j} - 2u_{i,j} + u_{i-1,j}}{h_x^2} + \frac{u_{i,j+1} - 2u_{i,j} + u_{i,j-1|}}{h_y^2} \tag{3.18}$$

This is an approximation of a Laplace operator and is called a 5-point stencily Higher point stencils can also be formed accompanied by higher accuracy but it also increases computation cost. Therefore 5-point stencil is used for spatial discretisation models.

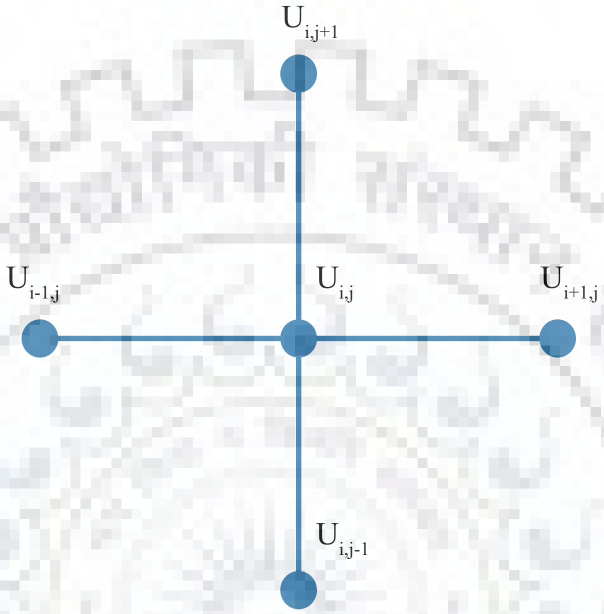

FIGURE 3.3: Five point stencil used in space discretisation

3.3.3 Finite Element Method

The finite element method like finite difference method used space domain discretization to map complex shapes using smaller, similar and manageable shapes. FEM can, however, describe complex geometries and boundary domain. In this method, any domain (1-D,2-D,3-D) is approximated using smaller predefined elements whose definition comes from basis or shape function. The underlying idea is that these elements individually are much easier to solve rather than the whole domain.

Elements and nodes

Let us divide the domain Ω in which the f and u are defined into non-overlapping subintervals E_i.In this domain let E_i be an element, having number i.We now introduce a set of points called Nodes where shape functions have a value of 1. These nodes are given numbers to define their positions both within an individual element and within the object. These are referred as local and global node number, respectively. In figure 3.4 three elements are shown with each element having three nodes. A total of seven nodes are there in the domain. Element E_1 extends from 0.1 on the x axis to 0.4 on the x axis. It has node points on 0.1, 0.25 and 0.4.

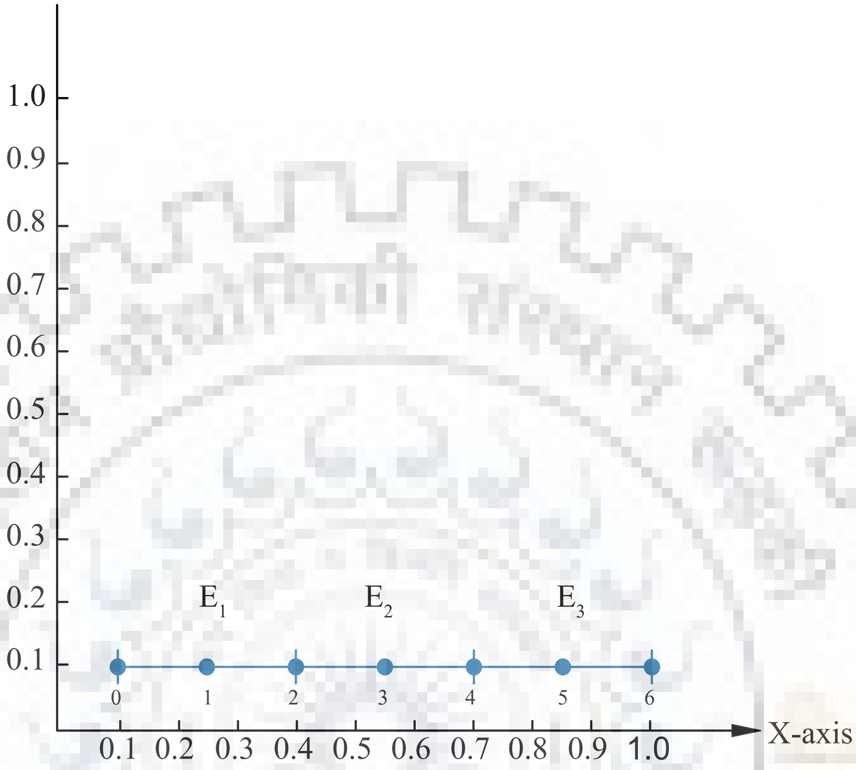

FIGURE 3.4: Figure representing nodes (blue circles) and elements (blue horizontal lines)

Isoparametric Representation

This representation is used to formulate a geometry of an element into simpler nodal unknowns like displacement. These nodal points or unknowns which combine to form a simple element. These nodal points have two types of co-ordinates, local and global. ζ and η localized co-ordinate system varying between -1 to 1 over an element.

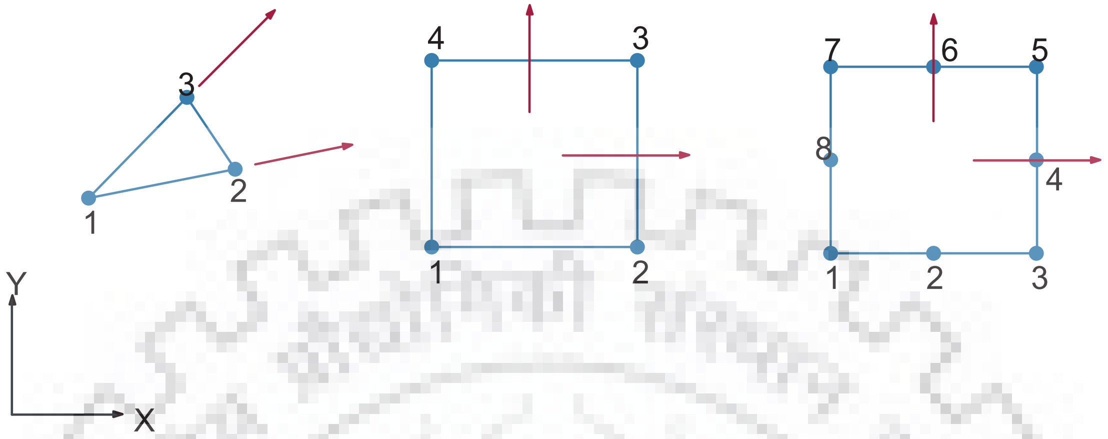

FIGURE 3.5: 1) Three node 2) Four node 3) Eight node Isoparametric representation of an element

Shape Functions

Shape functions are certain Langrangian of Legendre polynomial functions that are used to define the geometry of the element and node values. They have key characteristics as

1. Its value is 1 at node points and 0 every other node of the element
2. Its value is 0 over every element boundary not including ith node.

Nodes within an element are represented with x and y global co-ordinate and their representation in local co-ordinate through the use of isoparamertic formulism is

$$x(\zeta,\eta) = \sum_{i}^{n} N_i^e x_i^e \tag{3.19}$$

$$y(\zeta,\eta) = \sum_{i}^{n} N_i^e y_i^e \tag{3.20}$$

where n and N_i^e are number of nodes in an element and nodal values of shape function respectively.$\mathcal{X}_i^e$ and y_i^e are global co-ordinate values. In the figure 3.6 two simple polynomial shape function are shown. As can be seen they have value 1 at the node to which they belong and 0 on all other nodes.

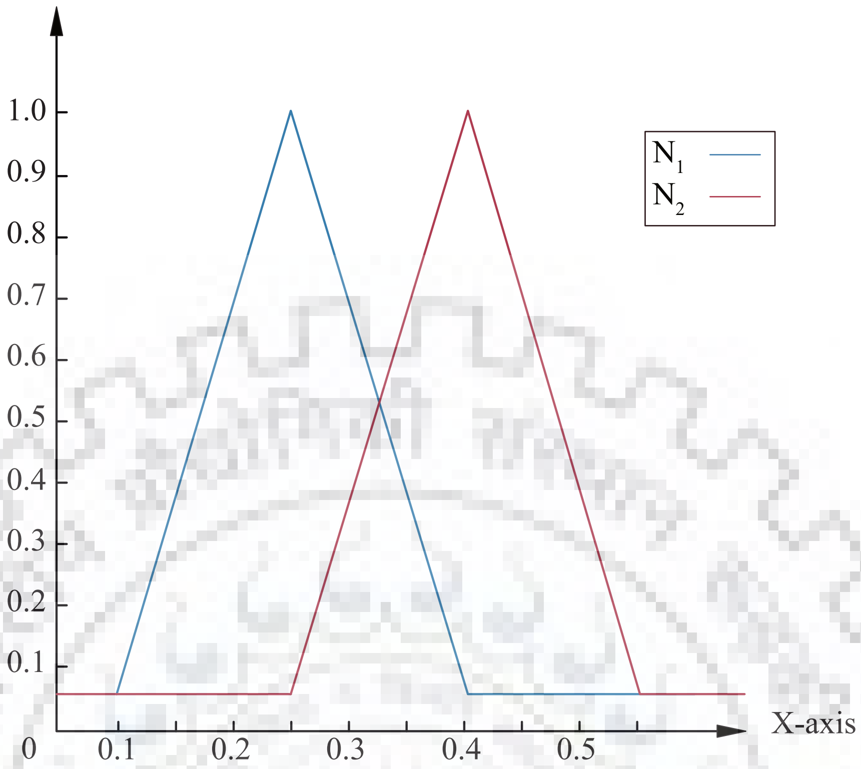

FIGURE 3.6: Simple linear shape functions

The displacement δ in any mechanical problem can be obtained from isoparameteic formulation by using shape functions as:

$$\delta = \begin{bmatrix} u \\ v \end{bmatrix} = N\delta^e = \sum_i^n N_i\delta_i \tag{3.21}$$

u is a displacement component in x direction and v in y direction in the Cartesian coordinate system. N_i and δ_i are shape function and nodal displacement respectively. Strain can be obtained from the nodal displacement derivatives:

$$\varepsilon = \begin{bmatrix} \varepsilon_{xx} \\ \varepsilon_{yy} \\ \varepsilon_{xy} \end{bmatrix} = \begin{bmatrix} \frac{\partial u}{\partial x} \\ \frac{\partial v}{\partial y} \\ \frac{\partial u}{\partial y} + \frac{\partial v}{\partial x} \end{bmatrix} \tag{3.22}$$

Inserting δ_i values from gg takes form of

$$\varepsilon = B\delta^e = \sum_{i=1}^n B_i\delta_i \tag{3.23}$$

B here is strain matrix defined as

$$B_i = \begin{bmatrix} \frac{\partial N_i}{\partial x} & 0 \\ 0 & \frac{\partial N_i}{\partial y} \\ \frac{\partial N_i}{\partial y} & \frac{\partial N_i}{\partial x} \end{bmatrix} \tag{3.24}$$

These derivatives are evaluated using Jacobian Matrix.

Chain rule and Jacobian

To find Cartesian derivative of a function f defined as

$$f(\zeta,\eta) = \sum_i^n N_i^e f_i^e \tag{3.25}$$

where f_i^e is nodal value of the function then the derivative of the function with respect to x and y are defined as

$$\frac{\partial f}{\partial x} = \frac{\partial f}{\partial \zeta} \cdot \frac{\partial \zeta}{\partial x} + \frac{\partial f}{\partial \eta} \cdot \frac{\partial \eta}{\partial x} \tag{3.26}$$

$$\frac{\partial f}{\partial y} = \frac{\partial f}{\partial \zeta} \cdot \frac{\partial \zeta}{\partial y} + \frac{\partial f}{\partial \eta} \cdot \frac{\partial \eta}{\partial y} \tag{3.27}$$

where $\partial f/\partial \zeta$ and $\partial f/\partial \eta$ are the shape function derivatives with respect to local co-ordinates and are given as

$$\frac{\partial f}{\partial \zeta} = \sum_i^n \frac{\partial N_i^e}{\partial \zeta} \cdot f_i^e \tag{3.28}$$

$$\frac{\partial f}{\partial \eta} = \sum_i^n \frac{\partial N_i^e}{\partial \eta} \cdot f_i^e \tag{3.29}$$

The values $\partial_\zeta/\partial x$,$\partial\eta/\partial x$,$\partial_\zeta/\partial y$ and $\partial\eta/\partial y$ to be used in the chain rule are found by forming a jacobian matrix and then inverting it.

$$J^e = \begin{bmatrix} \frac{\partial x}{\partial \zeta} & \frac{\partial y}{\partial \zeta} \\ \frac{\partial x}{\partial \eta} & \frac{\partial y}{\partial \eta} \end{bmatrix} = \begin{bmatrix} \sum_i^n \frac{\partial N_i^e}{\partial \zeta} \cdot x_i^e & \sum_i^n \frac{\partial N_i^e}{\partial \zeta} \cdot y_i^e \\ \sum_i^n \frac{\partial N_i^e}{\partial \eta} \cdot x_i^e & \sum_i^n \frac{\partial N_i^e}{\partial \eta} \cdot y_i^e \end{bmatrix} \tag{3.30}$$

The inverse of this matrix is then

$$[J^e]^{-1} = \frac{1}{\det J^e} \begin{bmatrix} \frac{\partial y}{\partial \eta} & -\frac{\partial y}{\partial \zeta} \\ -\frac{\partial x}{\partial \eta} & \frac{\partial x}{\partial \zeta} \end{bmatrix} \tag{3.31}$$

$\det J^e$ is the jacobain matrix's determinant.

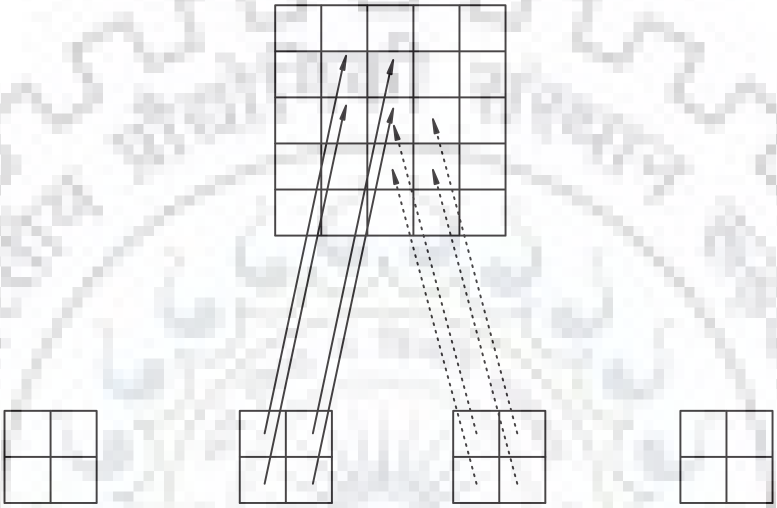

FIGURE 3.7: Process of formation of global stiffness matrix from element stiffness matrix

Chapter 4

Phase Field Modeling

4.1 Introduction

Phase field modelings origin can be traced in the microstructure evolution equation used to model microstructure or phases. These phases can be regions of different crystal orientations, different magnetic or electric domains. The solutions to these types of problems are classified as sharp interface approaches. These sets of non-linear problems are extremely difficult to solve, due to interactions between the interfaces arising from various complex processes during the phase transformation process. Phase field modeling was developed to overcome these difficulties by describing the boundary into a diffused region rather than a sharp one. It describes microstructures with a set of field variables which are diffused rather than being sharp in the region of the interface

4.2 Cahn Hilliard Equation

The origins of the Cahn-Hilliard model lies in a phase separation model known as spinodal decomposition, which is a solid state phase transformation in a binary alloy. Spinodal decomposition is a mechanism through which a solid solution decomposes into seperate phases having distinct compositions.. Unlike the nucleation driven mechanism which occurs at discrete location spinodal decomposition takes place throughout the material. The Cahn-Hilliard equation is given by

$$\frac{\partial c_i}{\partial t} = \nabla M_{ij} \nabla \frac{\delta F}{\delta e_j(r,t)} \tag{4.1}$$

In the equation 4.1 r and t are time and position respectively ,M_{ij} is diffusivity of the components c_1, c_2, c_n, which are conserved field variables.

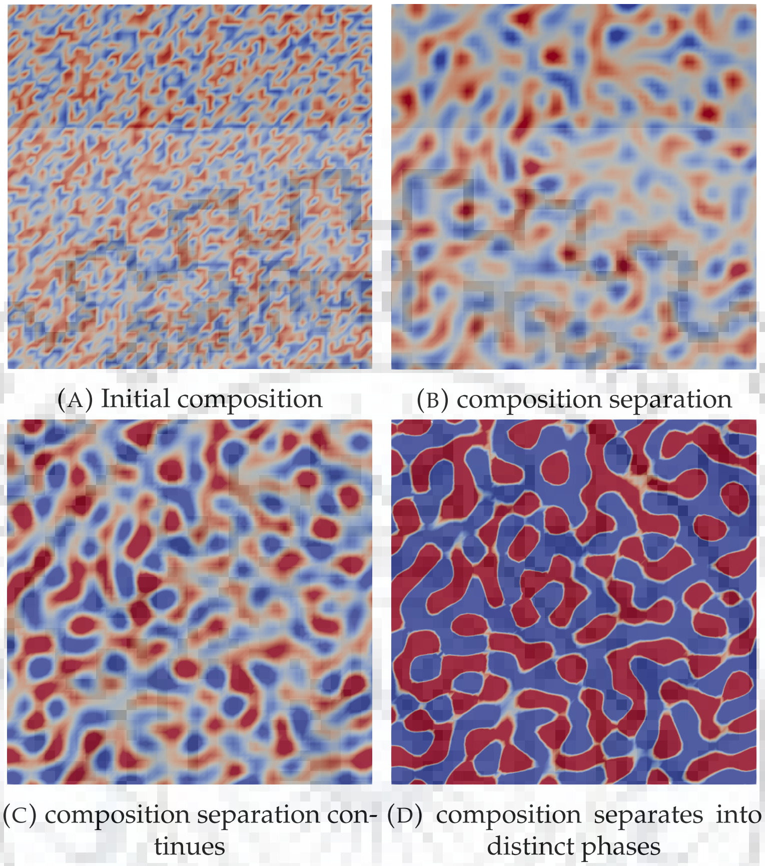
(A) Initial composition
(B) composition separation
(C) composition separation continues
(D) composition separates into distinct phases

FIGURE 4.1: Spinodal decomposition of binary alloy

4.3 Phase Field Derivation

Cahn and Hilliard derived a free energy partial differential expression for an inhomogeneous binary system taking the number of components in the equation 4.1 as two. Their primary assumption was that that total free energy of a very small region in a domain is equal to not only equal to the energy of its composition but also the composition of the environment which surrounds the small region. This is because they concluded that the total energy of the system not only depends on its concentration but also on its surroundings as a different spatial configuration having the same volume fraction have different energies i.e. they are not energetically equivalent.

Initially Cahn-Hilliard performed Taylor series expansion on homogeneous free energy density function for binary system in terms of the derivatives of the composition to obtain approximations of f $\left(\mathrm{c}, \nabla \mathrm{c}, \nabla^2 \mathrm{C}, \ldots\right)$. As concentrations here are binary they obey the rule $c_1 + c_2 = 1$, so only one concentration fraction in independent whichever that may be. Free energy equation for an isotropic system reduces to an expression containing constants and even power of ∇c as:

$$f = f_0(c) + \kappa_1 \nabla^2 c + \frac{1}{2}\kappa_2 (\nabla c)^2 + \frac{1}{2}\kappa_3 \left(\nabla^2 c\right)^2 + \kappa_4 \nabla^4 c + ... \tag{4.2}$$

They argued that even powers of the derivative terms should vanish, thus only first and second order terms remain,

$$F = \int_V \left[f(c) + \frac{1}{2}\kappa (\nabla c)^2 \right] dv \tag{4.3}$$

First term here represents chemical or bulk energy and is given by

$$f(c) = Ac^2 (1 - c)^2 \tag{4.4}$$

which is represented in a chemical energy vs concentration graph would give double wall potential phenomenon. k is a gradient energy coefficient which discourages formation of sharp boundary interfaces.

A is an amplitude controlling constant determining the depth of those potential controlling the barrier between the two equilibrium phases. Other double wall potential having similar characteristics exists, which can also be used.

4.3.1 Finite Element Implementation

Rearranging equation 4.1 we get,

$$\frac{\partial c}{\partial t} - \nabla \cdot M \left(\nabla \left(\frac{\partial f}{\partial c} - \kappa \nabla^2 c \right) \right) = 0 \quad \text{in } v \tag{4.5}$$

$$M \left(\nabla \left(\frac{\partial f}{\partial c} - \kappa \nabla^2 c \right) \right) = 0 \quad \text{in} \quad \partial v \tag{4.6}$$

$$M \kappa \nabla c \cdot n = 0 \quad \text{in} \quad \partial v \tag{4.7}$$

where v , ∂v and n are volume ,boundary and normal vector pointing outward.

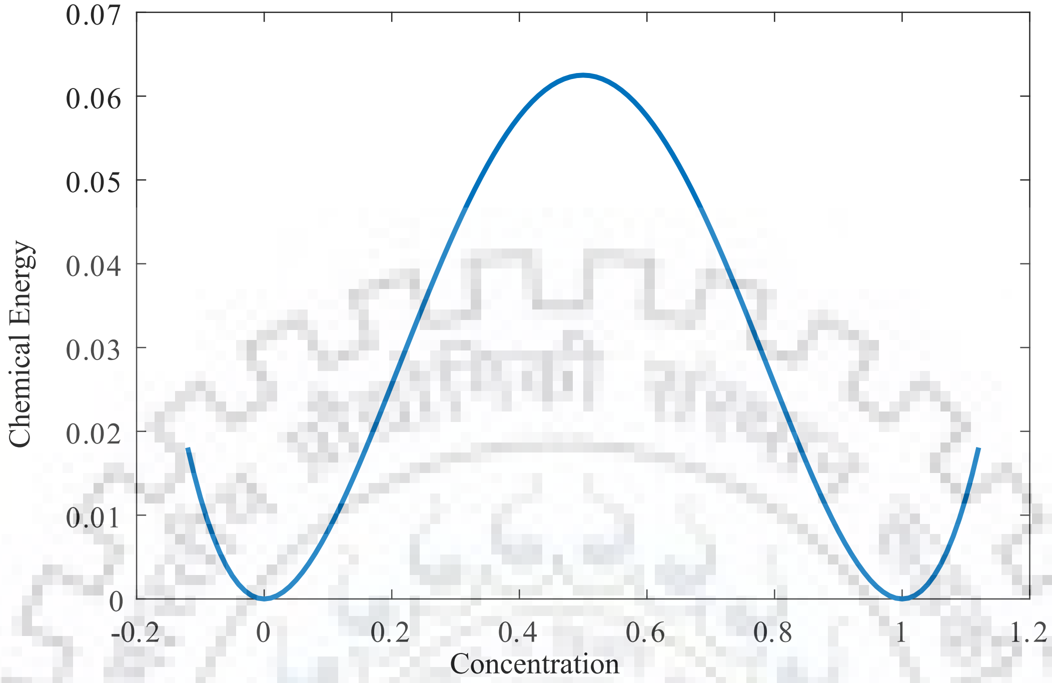

FIGURE 4.2: Double well potential

Due to the presence of the second and fourth-order spatial derivatives to change the equation into the weak form using test function will result in second-order spatial derivatives which would require higher-order shape function which will increase computational resources. Therefore the equations are converted into two coupled 2nd order equation which will become linear after changing to weak form. These are given as

$$\frac{\partial c}{\partial t} - \nabla \cdot M \nabla \mu = 0 \tag{4.8}$$

$$\mu - \frac{\partial f}{\partial c} + \kappa \nabla^2 c = 0 \tag{4.9}$$

The unknown to be solved now are c and μ. Utilizing the test function η ,ζ for c and μ respectively yields,

$$\int_v \frac{\partial c}{\partial t} \eta dv + \int_v M \nabla \mu \cdot \nabla \eta dV = 0 \tag{4.10}$$

$$\int_v \mu \zeta dv - \int_v \frac{\partial f}{\partial c} \zeta dv - \int_v \kappa \nabla c \cdot \nabla \zeta = 0 \tag{4.11}$$

Now applying implicit Euler time integration scheme discussed in chapter 3 gives

$$\int_v \frac{c^{n+1}-c^n}{dt}\eta dv + \int_v M\nabla\mu^n \cdot \nabla\eta dv = 0 \tag{4.12}$$

$$\int_v \mu^{n+1}\zeta dv - \int_v \frac{\partial f^{n+1}}{\partial c}\zeta dv - \int_v \kappa\nabla c^{n+1}\cdot\nabla\zeta dv = 0 \tag{4.13}$$

where $dt = t^{n+1} - t^n$ is time increment.

In this FEM implementation we take c, μ as nodal variables, and with the help of shape function they can be defined by

$$c = \sum_i^n N_i c_i \tag{4.14}$$

$$\mu = \sum_i^n N_i \mu_i \tag{4.15}$$

c_i , μ_i are the nodal values expressed using N_i as the shape function to define nodal values c and μ respectively, where n is the number of elements. Utilizing 4.14,4.15 the residual vector can be expressed as:

$$R_i^e = \int_V \begin{bmatrix} \left(c^{n+1}-c^n\right) N_i + dtM\mu^{n+1}\left(\frac{\partial N_i}{\partial x}\frac{\partial N_i}{\partial y}\right)^T \cdot \left(\frac{\partial N_j}{\partial x}\frac{\partial N_j}{\partial y}\right) N_j \\ \mu^{n+1}N_i - \frac{\partial f^{n+1}}{\partial c}N_i - \kappa c^{n+1}\left(\frac{\partial N_i}{\partial x}\frac{\partial N_i}{\partial y}\right)^T \cdot \left(\frac{\partial N_j}{\partial x}\frac{\partial N_j}{\partial y}\right) N_j \end{bmatrix} dV \tag{4.16}$$

where $(\partial N/\partial x \partial N/\partial y)$ is derivative of shape function in Cartesian coordinates. Element stiffness matrix arising from it is

$$K_{ij}^e = \frac{\partial R_i^e}{\partial c \text{ or } \partial\mu} = \begin{bmatrix} K_{ij}^{cc} & K_{ij}^{c\mu} \\ K_{ij}^{uc} & K_{ij}^{u\mu} \end{bmatrix} \tag{4.17}$$

The individual components given as,

$$K_{ij}^{cc} = \int_V \left[N_i^T \cdot N_j\right] dV \tag{4.18}$$

$$K_{ij}^{c\mu} = \int_V \left[dtM\left(\frac{\partial N_i}{\partial x}\frac{\partial N_i}{\partial y}\right)^T \cdot \left(\frac{\partial N_j}{\partial x}\frac{\partial N_j}{\partial y}\right)\right] dV \tag{4.19}$$

$$K_{ij}^{\mu c} = \int_V \left[-\frac{\partial^2 f}{\partial c^2} N_i^T N_j - \kappa \left(\frac{\partial N_i}{\partial x} \frac{\partial N_i}{\partial y} \right) \cdot \left(\frac{\partial N_j}{\partial x} \frac{\partial N_j}{\partial y} \right) \right] dV \tag{4.20}$$

$$K_{ij}^{\mu\mu} = \int_V \left[N_i^T N_j \right] dV \tag{4.21}$$

Having formed the stiffness and residual matrix for an element they are now assembled to form global stiffness matrix. A matrix containig residue known as RHS is also formed.

$$\left[K^G \right] \{ d\delta \} = \left\{ R^G \right\} \tag{4.22}$$

$d\delta$ is the unknown vector given by

$$d\delta = (dc_1, dc_2, \ldots, dc_N, \ldots, d\mu_1, d\mu_2, \ldots, d\mu_N) \tag{4.23}$$

4.4 Phase Field Model for fracture modeling

Bourdin et. al. put forward a varient of regularized variational formulation in which the scalar field variable ϕ is taken as the variable describing the crack geometry. The scalar field variable is used to approximate the sharp crack between the values 0 and 1 transforming it into a diffused crack topography.

The scalar field variable ϕ is given as

$$\phi = \exp\left(\frac{-|x-a|}{l_0} \right) \tag{4.24}$$

This gives the fracture surface energy as

$$\psi_s = \int_{\Sigma_p} \mathcal{G}_c \left[\frac{(\phi - 1)^2}{4\ell_0} + \ell_0 |\nabla \phi|^2 \right] d\Omega \tag{4.25}$$

where ℓ_0 is crack topology parameter, specifically controlling its width. If ℓ_0 tends to zero when this regularised approach will be converge to the variational formulation i.e. diffusive crack converges to discrete crack. In his formulation he penalised strain energy density to correct for the loss in material stiffness, which gives the strain energy density as

$$\psi_e = \int_{\Omega_p} \left(\phi^2 + \eta\right) \psi_e d\Omega \tag{4.26}$$

where η is a numerical convenience operator having a very small value. The total energy therefore is

$$\psi_t = \int_{\Omega_p} \left(\phi^2 + \eta\right) \psi_e d\Omega + \int_{\Omega_p} \mathcal{G}_c \left[\frac{(\phi - 1)^2}{4\ell_0} + \ell_0 |\nabla c|^2\right] d\Omega \tag{4.27}$$

To obtain crack evolution displacement field variable u and phase field variable ϕ are evolved taking into account the principle of global minimality.

A thermodynamically consistent phase field model was proposed by [33] to address the inadequacies of Bourdins regularised version. One important feature in his model was to ensure that crack only occurs when the tension was applied. For that they decomposed the elastic energy through spectral decomposition into two parts, positive and negative, corresponding to the direction of the applied stress. Thus he took only the positive part of the energy to make it certain that crack propagation occurs in tension only.

$$\psi_e = \psi_e^+ + \psi_{\mathrm{p}}^- \tag{4.28}$$

where ψ_e^+ and ψ_e^+ are given as

$$\psi_e^+ = \frac{1}{2}\lambda \left(\mathrm{tr}\left(\epsilon^+\right)\right)^2 + \mu\epsilon^+ : \epsilon^+ \tag{4.29}$$

$$\psi_e^- = \frac{1}{2}\lambda \left(\mathrm{tr}\left(\epsilon^-\right)\right)^2 + \mu\epsilon^- : \epsilon^- \tag{4.30}$$

Unlike Bourdin's mode which penalized the strain energy density, Miche's model only penalises the positive part of the energy density during crack evolution.

$$\psi_e = \left[(1-k)\phi^2 + k\right] \psi_e^+ + \psi_e^- \tag{4.31}$$

k is very small number preventing full degradation of elastic energy. Hence the approximated total energy if the body for regularized formulation will be given by

$$\Phi_t = \int_{\Omega_p} \left(\left[(1-k)\phi^2 + k\right] \psi_e^+ + \psi_e^-\right) d\Omega + \int_{\Omega_p} \mathcal{G}_c \left[\frac{(\phi - 1)^2}{4\ell_0} + \ell_0 |\nabla\phi|^2\right] d\Omega \tag{4.32}$$

The principle of energy balance states that internal and external energy rates should be equal, therefore $\dot{\Phi}_t = 0$

The length scale parameter as discussed above plays an important role in determining the crack topology, mainly its width. According to Welschinger,[4] length scale parameter can either be considered as a purely numerical parameter or as one which depends on material properties. If considered as a numerical factor then the smaller its value the better for accuracy purposes, although that increases computational resources required. For stability purposes however

$$\frac{l_0}{L} <= 0.01 \tag{4.33}$$

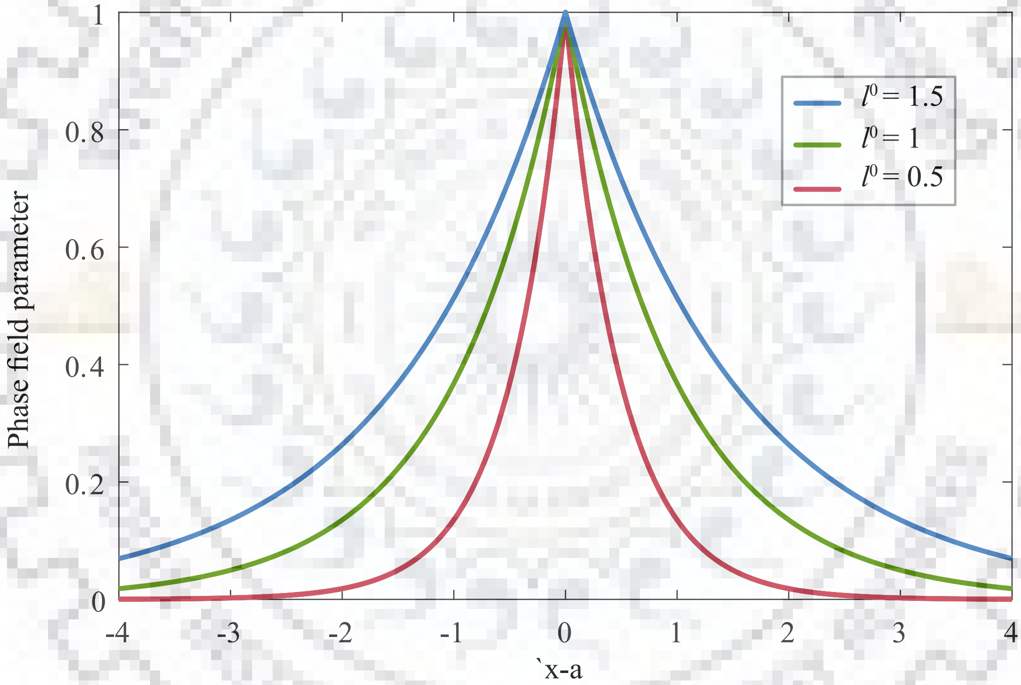

FIGURE 4.3: Figure representing the effect of length scale of the diffusive nature of the crack topology

As can be seen from the figure 4.3 lowering the value of length scale will cause the diffused crack geometry to be closer to the discrete geometry.

4.5 Phase Field Fracture FEM model

As stated in equation 4.27 in a body with a crack/damage the total potential energy is:

$$\Psi(\phi,u) = \int_V \left[(1-\phi)^2 + k\right]\psi(\varepsilon)dV + \int_V \frac{G_c}{2}\left[l_0\nabla\phi\cdot\nabla\phi + \frac{1}{l_0}\phi^2\right]dV \tag{4.34}$$

the first part of the equation represents strain energy change while second part represents decrease in energy due to formation of new crack surfaces. $\psi(e)$ here represents elastic strain energy

$$\psi(\varepsilon) = \frac{1}{2}\varepsilon C\varepsilon \tag{4.35}$$

where C and ε are elasticity matrix and strain respectively. Let incremental external work for equation 4.34 is δW_{ext}, its weak form is:

$$\delta W_{ext} = \int_V b_j\delta u_j dV + \int_{\partial V} h_j\delta u_j \partial V \tag{4.36}$$

b_j and h_j are body force and boundary traction components respectively. Change in internal energy is equal to internal work done and is given by

$$\delta W_{\mathrm{int}} = \delta\Psi = \frac{\partial\Psi}{\partial\varepsilon_{ij}}\delta\varepsilon_{ij} + \frac{\partial\Psi}{\partial\phi}\delta\phi \tag{4.37}$$

Applying equation 4.37 to 4.34 we get,

$$\delta\Psi = \int_V \left[(1-\phi)^2 + k\right]\sigma_{ij}\delta e_{ij}dV + \int_V -2(1-\phi)\delta\phi\psi(\varepsilon)dV + \int_V G_c\left(l_o\frac{\partial\phi}{\partial x_i}\frac{\partial\phi}{\partial x_i} + \frac{1}{l_0}\phi\delta\phi\right)dV \tag{4.38}$$

where δ is a test function. For finite element formulation we take displacement u and order parameter ϕ as nodal variables, u, $\nabla\phi$, ϕ and ε are descritized at elemental level:

$$u = |\sum_i^n N_i u_i, \varepsilon = \sum_i^n B_i^u u_i \tag{4.39}$$

$$\phi = \sum_i^n N_i\phi_i, \nabla\phi = \sum_i^n B_i^\phi \phi_i \tag{4.40}$$

where n denotes node numebers. B_i^u is the strain matrix and B_i^ϕ is the Cartesian derivative matrix.

$$B_i^u = \begin{bmatrix} \frac{\partial N_i}{\partial x} & 0 \\ 0 & \frac{\partial N_i}{\partial y} \\ \frac{\partial N_i}{\partial y} & \frac{\partial N_i}{\partial x} \end{bmatrix}, B_i^\phi = \begin{bmatrix} \frac{\partial N_i}{\partial x} \\ \frac{\partial N_i}{\partial y} \end{bmatrix} \tag{4.41}$$

As internal work done is equal to external work done (energy) the residue R_e^u for an element takes the form:

$$R_e^u = \int_V \left[(1-\phi)^2 + k\right] (B_i^u)^T \sigma dV - \int_V N^T b dV - \int_{\partial V} N^T h \partial V \tag{4.42}$$

T stands for transpose. The residual vector for equation 4.38

$$R_e^\phi = \int_V G_c l_0 \left(B_i^\phi\right)^T \nabla\phi + \left(\frac{G_c}{l_0} + 2\psi(\varepsilon)\right) N\phi - 2N\psi(\varepsilon)]dV \tag{4.43}$$

We form the stillness element matrix for Cahn-Hilliard equation 4.17 , in a similar way a stiffness matrix for for the residual vectors is formed as

$$K_e = \begin{bmatrix} K_{ij}^{uu} & K_{ij}^{u\phi} \\ K_{ij}^{\phi u} & K_{ij}^{\phi} \end{bmatrix} \tag{4.44}$$

.

The individual components are given as

$$K_{ij}^{uu} = \frac{\partial R_e^u}{\partial u} = \int_V \left[(1-\phi)^2 + k\right] (B_i^u)^T C B_j^u dV \tag{4.45}$$

$$K_{ij}^{u\phi} = \frac{\partial R_e^u}{\partial \phi} = \int_V -2(1-\phi) (B_i^u)^T \sigma N_j dV \tag{4.46}$$

$$K_{ij}^{\phi u} = \frac{\partial R_e^\phi}{\partial u} = \int_V -2(1-\phi) N_i \sigma B_j^u dV \tag{4.47}$$

$$K_{ij}^{\phi\phi} = \frac{\partial R_e^\phi}{\partial \phi} = \int_V \left[G_c l_0 \left(B_i^\phi\right)^T B_j^\phi + \left(\frac{G_c}{l_0} + 2\psi(\varepsilon)\right) N_i N_j\right] \tag{4.48}$$

Forming the stiffness and residual matrix, global stiffness matrix is formed by assembling them along with an right hand side vector , which results as

$$\left[K^G\right] \{\delta\} = \left\{R^G\right\} \tag{4.49}$$

Barrier term

The equations defined here do not explicitly ensure irreversibility condition, ie the fracture does not heal once the strain is removed ($\phi_{t+\Delta t} < \phi_t$). To overcome this problem the equations are subjected to an energy barrier condition described below

$$\langle x \rangle_- = \begin{Bmatrix} -x, & x < 0 \\ 0, & x \geq 0 \end{Bmatrix} \tag{4.50}$$

A barrier function is created from this definition given as

$$P(\dot{\phi}) = \eta \langle \dot{\phi} \rangle_- \tag{4.51}$$

η here represents the numerical value of the barrier preventing crack healing. Its value is assumed to be two times the elastic modulus of graphene.

भारतीय प्रौद्योगिकी संस्थान रुड़की
INDIAN INSTITUTE OF TECHNOLOGY ROORKEE

Chapter 5

Molecular Dynamics

5.1 Introduction

Molecular dynamics has emerged as an indispensable tool for studying material science at the atomic and molecular level. Studying molecules at the atomic level helps us get valuable insight into material behavior as well as predict new materials. It uses newtons second law to calculate the positions and velocities of a system of particles from its initial conditions.A variety of thermodynamic properties pertaining to the system can be obtained through it. Molecular Dynamics simulation consists of iterative solution of classical equations of motion, which for a system of particles can be represented as

$$m_i \ddot{\boldsymbol{r}}_i = \boldsymbol{f}_i \quad \boldsymbol{f}_i = -\frac{\partial}{\partial \boldsymbol{r}_i}\mathcal{U} \tag{5.1}$$

5.2 Interatomic Interaction

There are various component of total potential energy of a system. The part of potential energy which represent non bonded interactions (U non-bonded) between atoms is comprised of 1-body, 2-body and multibody interaction terms:

$$U_{\text{non- boncd}}\left(r^N\right) = \sum_i u\left(\boldsymbol{r}_i\right) + \sum_i \sum_{j>i} v\left(\boldsymbol{r}_i, \boldsymbol{r}_j\right) + \ldots \tag{5.2}$$

The one body interaction term $u(r)$ is the effect of boundaries on the system, it is generally ignored if the system being simulated is a periodic system. At is also typical to only focus on pair potential and ignore higher order interactions.

When talking about pair-wise potential Lennard-Jones potential is the simplest and also the most commonly used potential. It is of the form

$$v^{\mathrm{LJ}}(r) = 4\varepsilon\left[\left(\frac{\sigma}{r}\right)^{12} - \left(\frac{\sigma}{r}\right)^{6}\right] \tag{5.3}$$

where σ is the distance of neutral force and ε is the potential well depth.

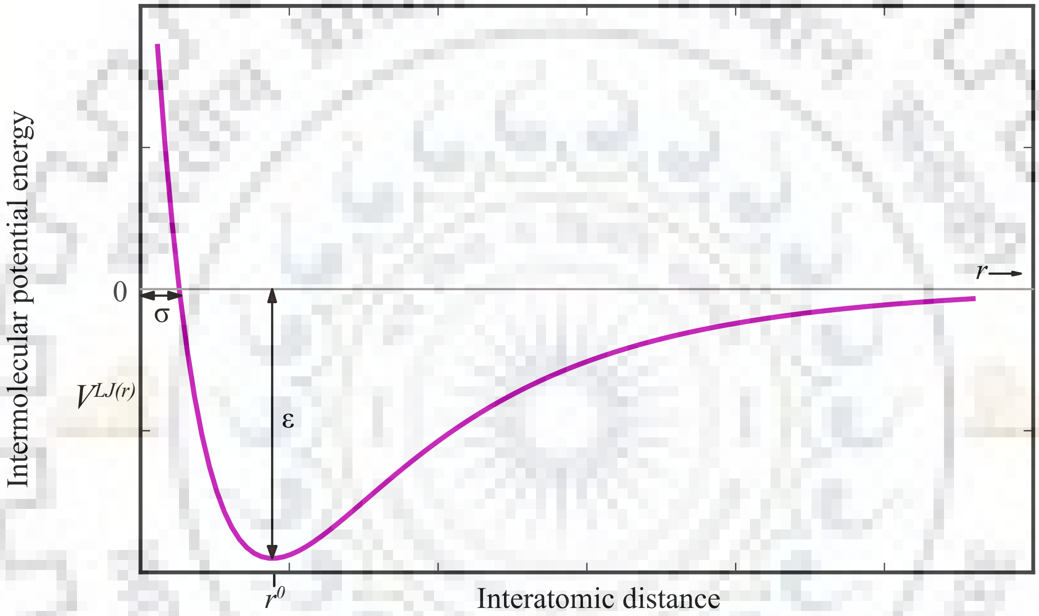

FIGURE 5.1: Interatomic potential vs interatomic distance

In case of the presence of electric charge a coulomb potential is used which is given by

$$v^{\text{Coulomb}}(r) = \frac{Q_1 Q_2}{4\pi\epsilon_0 r} \tag{5.4}$$

where Q_1 and Q_2 are charges on two atoms and $\in_0$ is the free space permtivity. Lennard-Jonnes potential is used to model short range potental such as Van-der Waal interaction between atoms while Coulomb interaction is used for long range interactions. As the Van-der Waal interactive force between atoms becomes very low at long ranges it is convenient to have a cut off after which the interactive force is assumed to be zero. This saves computational resources albiet at the expance of some accuracy.

For our simulation, we used AIREBO Stuart et al.[41] style pair potential. It stands for Adaptive Intermolecular Reactive Empirical Bond Order (AIREBO) Potential and computes system a system of carbon and/or hydrogen atoms. The AIREBO potential consists of 3 terms:
E_REBO is an original stand-alone potential developed by Brenner. This part of the potential describes short-range interactions (r < 2 Angstroms)between C-C, C-H and H-H atoms. It also gives the model developed, its reactive capabilities. These interactions are strongly dependent on the number of atoms nearby which is given by a bond order parameter that depends on the coordination number. thus this potential can be perceived as a multi-body potential..
E_LJ term simulates the longer ranged Van Der Waals forces ranging from 2 Angstrom to the specified cutoff. It uses the standard form of Lennard-Jones Potential. The lj term contains switching functions so that the repulsion term in the lj equation does not interfare with REBO term in the potential.
E_TORSION term is a 4-body potential that describes those dihedral angles which are preferred in the configuration so that the movement other then the dihedral angles are restricted.

5.3 Integration algorithm

As potential energy of a system depends on relative position, velocities and accelerations of all the particles of the system, it is therefore difficult to analytically calculate potential energy. For this reason numerical techniques and algorithm are needed. Main component of these algorithm is the approximation of position, velocities and acceleration by Taylor series expansion.

$$r(t+\delta t) = r(t) + v(t)\delta t + \frac{1}{2}a(t)\delta t^2 + \dots \tag{5.5}$$

$$v(t+\delta t) = v(t) + a(t)\delta t + \frac{1}{2}b(t)\delta t^2 + \dots \tag{5.6}$$

$$a(t+\delta t) = a(t) + b(t)\delta t + \dots \tag{5.7}$$

The postion ,velocity, acceleration for the next time steps are calculated using the above apprximations. Some common integration algorithms are Varlet algorithm, Velocity verlet, Leap-from algorithm.
The choice of algorithm is based on the following criteria:

1. Energy and momentum is to be conserved

2. Computational efficincy
3. Time step ahoultd be as long as possible

The Varlet Algorithm

This is the basic algorithm most commonly used for time intergation A very simple idea is implemented in order to find position of the particle in the next time step. Taylor expansion is carried out for $\mathbf{r}(t+\Delta t)$ and $\mathbf{r}(t-\Delta t)$ and added to get the expression for position at next time increment $\mathbf{r}(t+\Delta t)$

$$\mathbf{r}(t+\Delta t) = \mathbf{r}(t) + \mathbf{v}(t)\Delta t + (1/2)\mathbf{a}(t)\Delta t^2 + (1/6)\mathbf{b}(t)\Delta t^3 + O\left(\Delta t^4\right) \tag{5.8}$$

$$\mathbf{r}(t-\Delta t) = \mathbf{r}(t) - \mathbf{v}(t)\Delta t + (1/2)\mathbf{a}(t)\Delta t^2 - (1/6)\mathbf{b}(t)\Delta t^3 + O\left(\Delta t^4\right) \tag{5.9}$$

Adding 5.8 and 5.9 we get

$$\mathbf{r}(t+\Delta t) = 2\mathbf{r}(t) - \mathbf{r}(t-\Delta t) + \mathbf{a}(t)\Delta t^2 + O\left(\Delta t^4\right) \tag{5.10}$$

Acceleration is found using the newtons second law as

$$\mathbf{a}(t) = -(1/m)\nabla V(\mathbf{r}(t)) \tag{5.11}$$

where ∇V is the gradient of potential energy. The trancation error is in the order of Δt^4 . Therefore in time evolving equations it is used very often. One problem with this algorithm is that velocity is not directly found , so we have to compute it through poaitions using

$$\mathbf{v}(t) = \frac{\mathbf{r}(t+\Delta t) - \mathbf{r}(t-\Delta t)}{2\Delta t} \tag{5.12}$$

but in this case error increses to Δt^2. This causes deviation in predicted trajectories of the particles creating deviations from actual path of the particles. To overcome this error various different integrtion algorithm have been proposed amongst whome velocity varlet is the most commonly used. In our molecular dynamics simulation we have also used the same algorithm thus it is explained further.

The Velocity Varlet Algorithm

In this algorithm the position ,velocityand acceleration at time $t + \Delta t$ are obtained from the corrosponding quantities at time t as

$$\mathbf{r}(\dot{k} + \Delta t) = \mathbf{r}(t) + \mathbf{v}(t)\Delta t + (1/2)\mathbf{a}(t)\Delta t^2 \tag{5.13}$$

$$\mathbf{v}(t + \Delta t/2) = \mathbf{v}(t) + (1/2)\mathbf{a}(t)\Delta t \tag{5.14}$$

$$\mathbf{a}(t + \Delta t) = -(1/m)\nabla V(\mathbf{r}(t + \Delta t)) \tag{5.15}$$

$$\mathbf{v}(t + \Delta t) = \mathbf{v}(t + \Delta t/2) + (1/2)\mathbf{a}(t + \Delta t)\Delta t \tag{5.16}$$

5.4 Statistical mechanics

One of the main components of molecular dynamics in statistical mechanics. The information generated by molecular dynamics simulations represents atomic positions, velocities, temperature, etc. This information needs to be interpreted into macro scale properties for usability point of view which requires statistical mechanics. That is to say that if one wishes to study macroscopic properties obtain by the simulation one needs to know through statistical mechanics formulas how these atomic simulations translate to macroscopic properties.

It consists of mathematical expressions that relate macroscopic properties such as temperature, pressure, etc to the motion and distribution of atom across the system. It also provides a means to study both kinetic and thermodynamic properties by evaluating equations of motion. In order to provide a useful link between macroscopic and microscopic model, some definitions have to be clarified.

A thermodynamic state of a system is defined by a set of parameters eg temperature T, pressure P, energy E, and number of particles N. As these parameters can vary there can be infinite state in which a system can exist. It is possible that macroscopically a system can have the same state but microscopically they can have a large number of states. Taking this into account a term ensemble is defined which is a collection of microscopic states which have the same macroscopic states.

5.5 Ensemble

Different Kinds of Thermodynamic ensemble exists depending on the macroscopic properties taken. Some of these properties are made to be constant while others are allowed to vary as the system is allowed to evolve. Some commonly used ensembles are defined below:

1. Canonical Ensemble (NVT) This state is characterized by having the number of atoms N fixed, volume V temperature T fixed.
2. Isobaric-Isothermal Ensemble(NPT) This has a fixed number of atoms N, fixed pressure$P$ and fixed temperature T.
3. Microcanonical Ensemble(NVE) This is essentially a closed system, in which the energy E is constant rather than temperature and volume.

5.6 Perodic Boundary Conditions

As the sample size becomes decreases, the percentage of atoms residing at its surface increases. For example, a solid sample of 10^6 atoms arranged in a simple cubical manner has around 6% atoms on its surface, but for the sample size of 1000 atoms arranged similarly the percentage is around 50%. It is also known that the free surface contains energy due to the unbounded nature of the surface atoms. It is due to this fact that small sample may show properties that are different than their bulk counterparts. In order to then study bulk properties in molecular dynamics, the sample is surrounded by replicas or images of itself. To prevent atoms from interacting with the same atom or its image twice we use minimum image convention, i.e the interaction happens only between nearest atom or image. As seen in figure 5.2, if an atom leaves the simulation box then the atom which was interacting with it will now be interacting with its image entering the simulation box. For long range potential this might cause a problem as atoms might interact with an infinite number of image, so careful considerations has to be made.

5.7 Molecular Dynamics simulation algorithm

Each step in molecular dynamics simulation follows a particular algorithm from the start of the timestep to its end. A time step is the distance between two points in time where position, acceleration, velocities and other quantities are calculated. The smaller the time

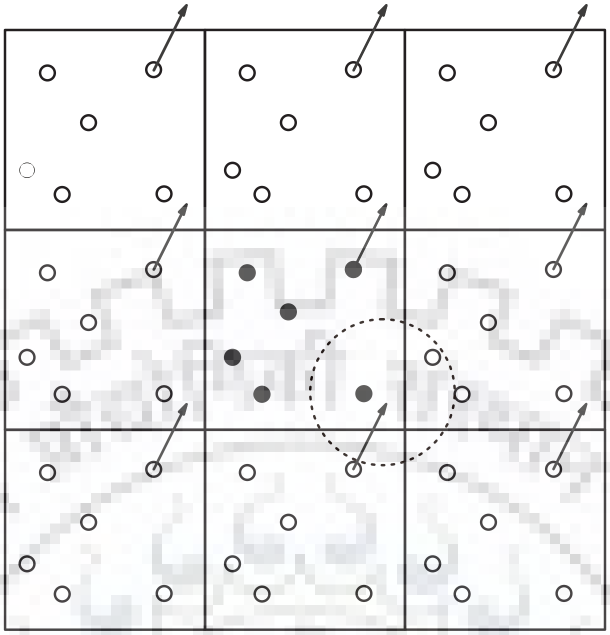

FIGURE 5.2: Figure representing periodic boundary with main simulation cell in centre and its image surrounding it. When an atom leaves the periodic boundary its image enters the simulation cell from other side.

step the more accurate the simulation trajectory is. However smaller timesteps may cause a significant increase in the time it takes for a simulation to be performed. As a general rule of thumb, the time step should be smaller than the frequency of the fastest bond in the molecule. Here is a flowchart depicting the algorithm.

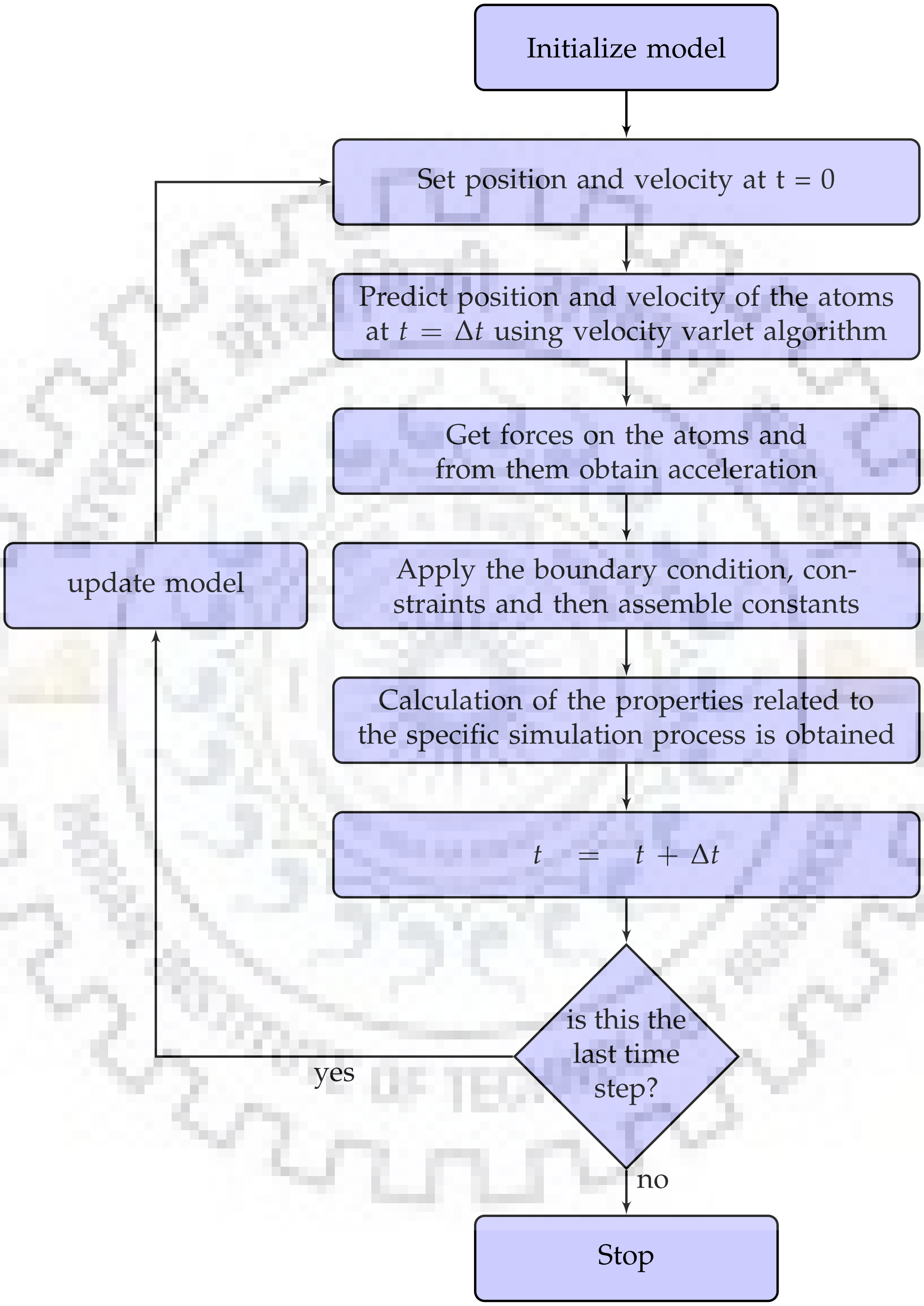
Initialize model
Set position and velocity at t = 0
Predict position and velocity of the atoms at $t = \Delta t$ using velocity varlet algorithm
Get forces on the atoms and from them obtain acceleration
Apply the boundary condition, constraints and then assemble constants
Calculation of the properties related to the specific simulation process is obtained
$t = t + \Delta t$
is this the last time step?
yes
no
update model
Stop

FIGURE 5.3: Molecular dynamics algorithm

Chapter 6

Simulation

6.1 General

In this chapter, molecular dynamics simulation of fracture in a single layer graphene sheet is performed. Mechanical properties are obtained through a number of these simulations which are then used to performing phase field fracture given in chapter 7 from the model presented in chapter 4. The two results are then compared and similarities are pointed out.

6.2 Molecular Dynamics

Single layer graphene sheet was selected as the material to be used in the fracture simulation. SGLS is a two dimensional material due to which a relatively large dimension can be simulated with limited computational resources. Secondly, SGLS is brittle in nature making it the perfect candidate for the selection. The graphene sheet was constructed using a crystallographic information file (CIF) in enCIFer topography software. A sheet of graphene was then generated using VMD with dimensions of 20nm x 10nm containing 8000 carbon atoms. The simulation was run in by Large-scale Atomic/Molecular Massively Parallel Simulator (LAMMPS). The interatomic potential used in an AIREBO discussed in section 5.2 with a cut-off for LJ part being 10.3 nm. The cut off for the REBO part of the potential for carbon-carbon bonds were changed from 1.7 to 1.92 to eliminate non-physical behavior [7] of c-c bonds when subjected to high strain as in the case with fracture, as suggested by the studies.[37].

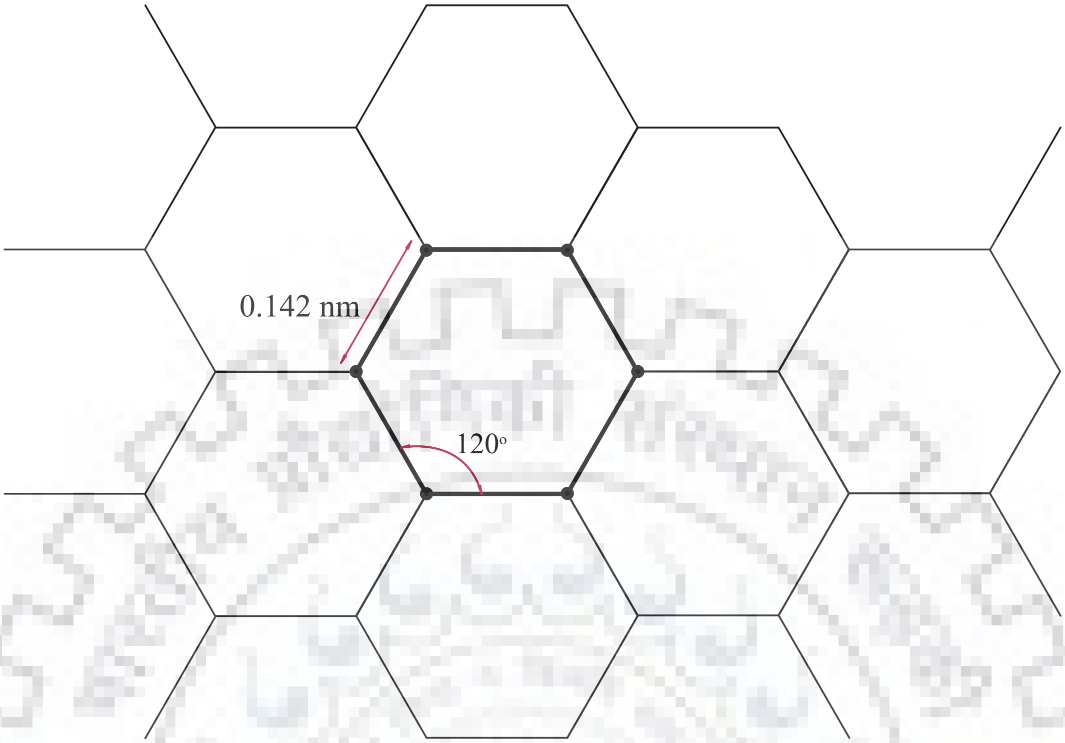

FIGURE 6.1: Graphene structure

Before running fracture simulations the graphene sheet is minimized and equilibrated in an NPT ensemble at 300 k for 15000-time steps with each time step being 0.5 femtoseconds for added accuracy. No change in structure was observed and the fluctuations in temperature and energy were quickly stabilized as shown in figure 6.3 and 6.4 establishing a stable structure. The final frame of the simulation was used as the final model for this simulation.

Two simulations were performed to gather all the parameters needed for the phase field simulations. In the first simulation, the ultimate fracture strength was the parameter to be found. A crack geometry was introduced in the graphene sheet using delete atom functionality of LAMMPS, which deletes a group of atom defined by the user. A simulation cell boundary was introduced which were periodic in X and Y direction but shrink-wrap in Z direction to compensate for the folding and wrinkling phenomenon observed during the deformation process. A 2-angstrom gap between graphene layer x directions and the cell boundary were given so that surface effects can take place. To perform the fracture stimulation the graphene sheets layer was fixed at the edges to the simulation cell which was then expanded at a constant strain rate of 10 nm ns^{-1}. This would be equivalent to a MODE I fracture in which the load applied is perpendicular to the crack path. The load

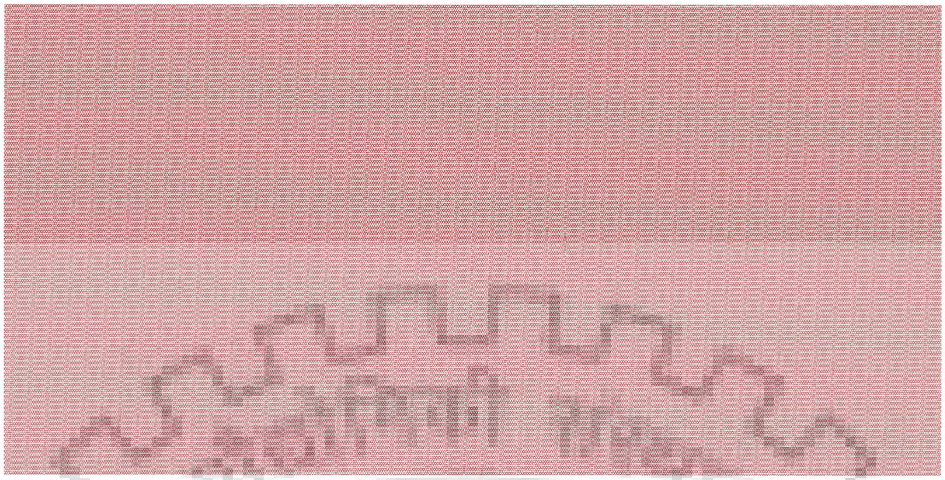

FIGURE 6.2: Graphene sheet

here is applied in the X axis while the crack is free to move in y direction.

In accordance with the goal to capture the fracture strength of the SGLS a stress-strain graph was to be formed. Stress was calculated by multiplying the summed stress output by corrected volume in which the thickness of the sheet was taken as 0.34 nanometre. The strain is given by simply multiplying the strain rate with the number of time steps.

The second simulation was run to obtain the elastic constant also known as Young's modulus and Poisson's ratio. The sample model of 5nm$x$5nm, 10nm$x$10nm and 20nm$x$20nm were created with periodic boundary conditions in two dimensions. These simulations were run for 50000 time steps with the same strain rate as the previous run. This gives relatively linear and smooth elastic characteristics which makes it easier to obtain those properties. The elastic modulus is obtained from the stress-strain graph while Poisson's ratio is obtained as

$$\nu = -\frac{\varepsilon_x}{\varepsilon_y} \tag{6.1}$$

where ε_y is strain in y direction while ε_x is strain in x-direction.

6.3 Phase field simulation

Following the FEM implementation of the phase-field fracture the model is implemented as code in MATLAB software because of its ease of coding and excellent vector, matrix function library. As can be seen in figure 6.7 FEM mesh was generated with 4141 nodes

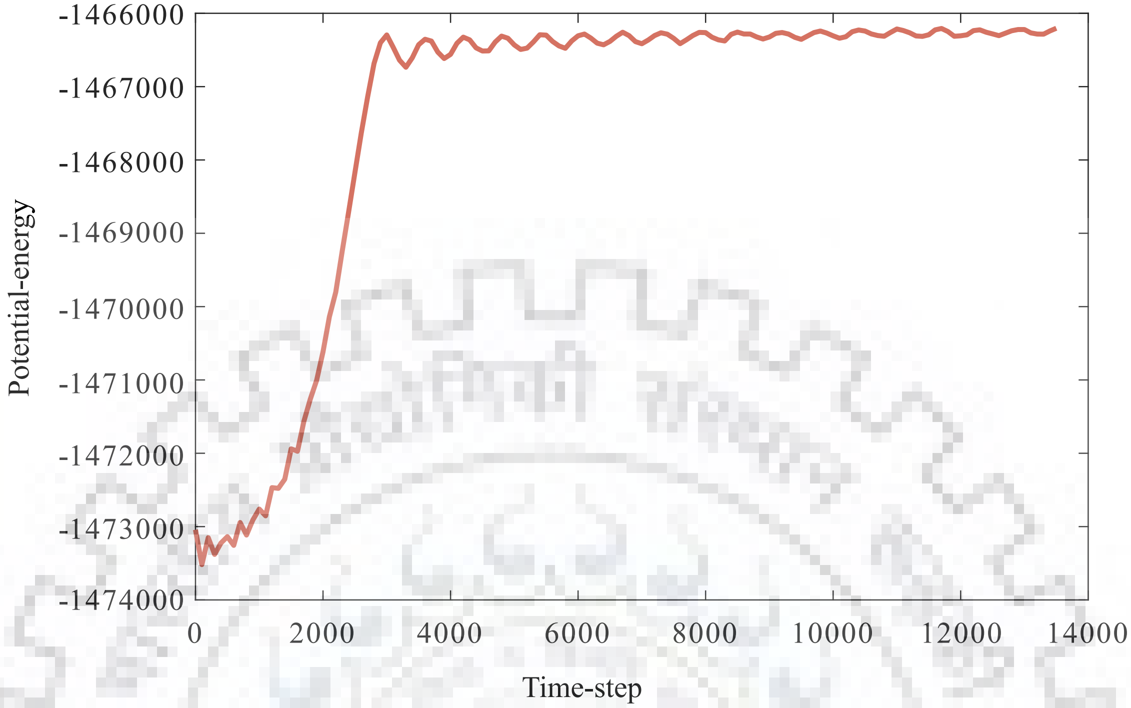

FIGURE 6.3: Stabilization of potential energy

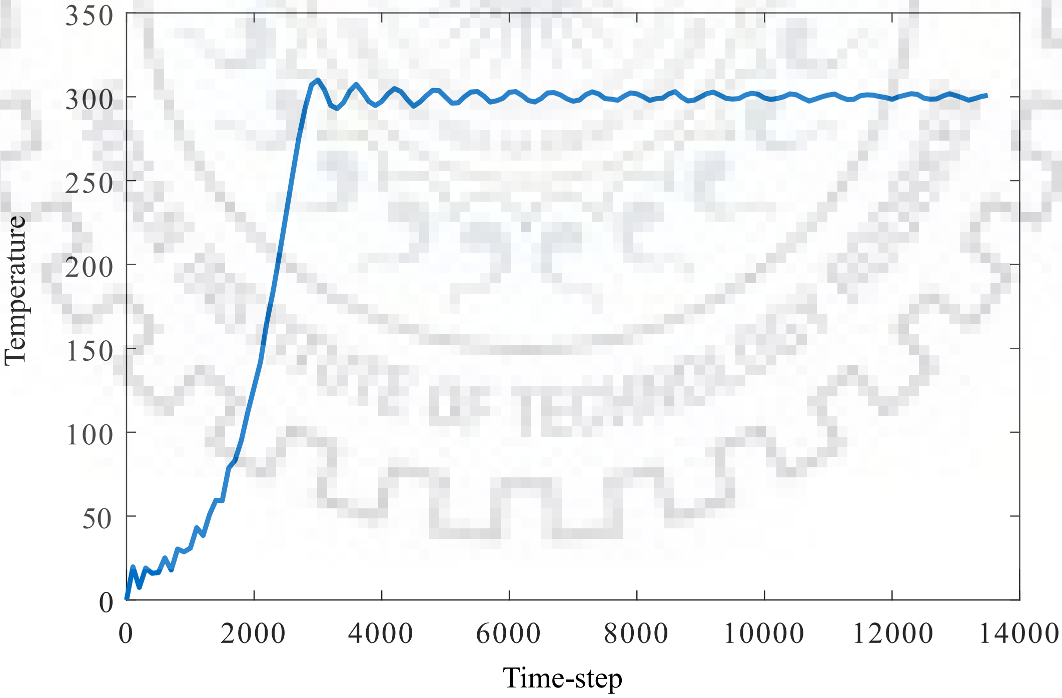

FIGURE 6.4: Stabilization of temperature

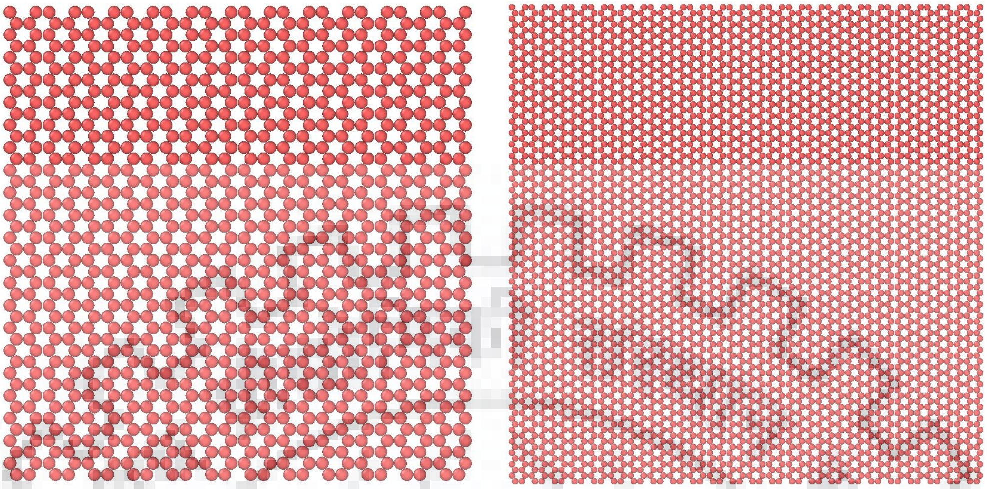

(A) 5nm graphene sheet

(B) 10nm graphene sheet

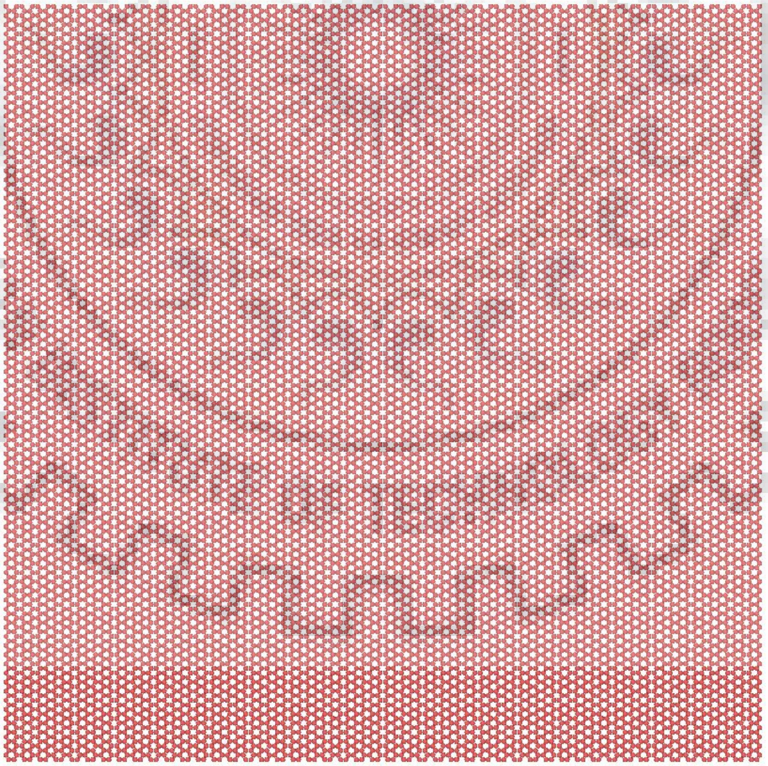

FIGURE 6.6: 20nm graphene sheet

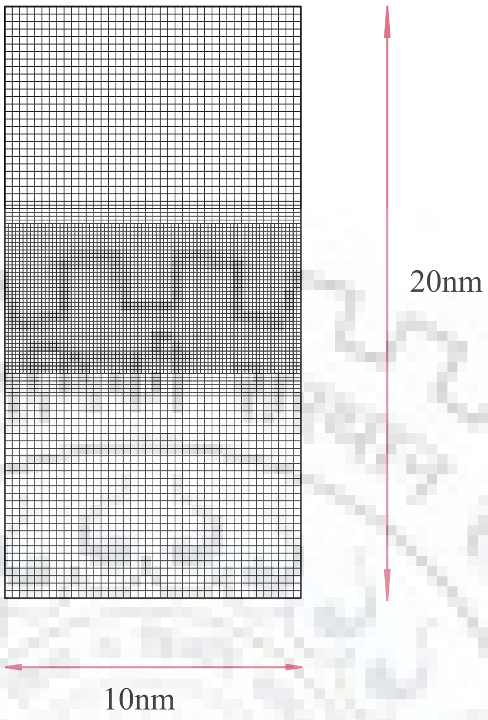

FIGURE 6.7: Finite element mesh

and 4000, four-node isoparametric elements with the dimensions of 50nm *x* 100nm. The crack was introduced manually with a crack array.

Chapter 7

Results and Discussion

7.1 General

In this chapter results from the simulation performed in the previous are reported and discussed as to what they suggest. They will be further analyzed and compared to each other and report any correlation in the phase field parameter and physical nature.

7.2 Molecular Dynamics

In the first simulation, each graphene sheet with different sizes was run until small deformation was observed. The deformations were small and were within the elastic region.

Simulation results

The following results were obtained for different size sheets. For calculating Poisson's ratio and elastic modulus using we use the formulas

Sheet Size	Initial length Lo	Length at 2% strain L	Initial width Xo	Final width X
5nm x 5 nm	5.077931	5.1794928	5.0298703	5.0078424
10nm x 10 nm	10.168647	10.37202	10.06383	10.013558
20nm x 20 nm	20.097614	20.499566	20.125827	20.029058

TABLE 7.1: Change in dimensions in the graphene sheets under uniaxial tension

$$\nu = -\frac{\varepsilon_x}{\varepsilon_y} = -\frac{X - X_0}{L - L_0} \tag{7.1}$$

where ε_y is strain in y direction while ε_x is strain in x direction. Similarly elastic modulus is given by

$$E = \frac{Stress}{strain} = \frac{\sigma}{\varepsilon} \tag{7.2}$$

Using the data given in the table 7.1 and using equations 7.1 and 7.2 we get the Poisson's ration and Young's modulus as

Sheet size	**Stress at 2% strain**	**Lateral strain**	**Poisson's ratio**	**Young's modulus**
5nm x 5nm	16.966384	0.004379	0.2169	848 GPa
10nm x 10nm	18.117726	0.004995	0.24721	906 GPa
20 nm x20 nm	18.224222	0.004808	0.2398	911 GPa

TABLE 7.2: Mechanical properties derived from the results

Reference	**Simulation method**	**Elastic Modulus (GPa)**	**Poisson's ratio**
Liu et al.[31]	DFT	1050	0.186
Kudin et al[27]	DFT	1029	0.149
Sanchez-Portal[6]	DFT	1070	0.14-0.19
Gupta[21]	MD (Brenner potential)	1272	0.147
Chang[15]	MM (Morse potential)	1060	0.16
Zhao[23]	MD (AIREBO)	1010 ± 30	0.21 ± 0.01
Lu[32]	MD (REBO)	725	0.398
Wei[43]	DFT	1039	0.169
Pei[36]	MD (AIREBO)	893	-
Cadelano[12]	TB	931	0.31
Reddy[38]	MM (Tersoff–Brenner)	669	0.416

TABLE 7.3: Mechanical properties of graphene derived in available literature

As can be seen from table 7.3 the results obtained are in line with the previous studies. The results vary from 1272 to 725 GPa for elastic modulus while 0.14 to 0.416 for Poisson's ratio, making our results sit right in between the range of results. However, for molecular dynamics simulation studies using AIREBO potential, the elastic modulus and poisons are very close to the previous studies from Zhao and Pei as can be seen from the table 7.3. The averages of these are taken as 888.88 GPa for Elastic modulus and 0.234 as Poisson's ratio.

A second simulation in which a constant strain rate uniaxial tensile test was performed on the graphene sheet of dimension 20nm x 10nm. As stated before the purpose of this simulation is to obtain critical energy release rate G_c which is an important component for our phase field simulation.

According to the Griffith's criterion of fracture of brittle material as discussed in 3.2 is given by

$$\sigma_f = \frac{1}{\alpha}\left[\frac{2E\gamma}{\pi a}\right]^{1/2} \tag{7.3}$$

where σ_f is the stress at fracture , γ and a are surface energy and one-half notch depth respectively. α is a geometry correction factor and for a single edge crack in a thin sheet and is equal to 1.12. Using this equation G_c can be calculated as being equal to twice of γ. G_c can also be calculated by integrating the stress strain curve with respect to strain $\mathcal{E}$ given by

$$G = l\int \sigma(\varepsilon)d\varepsilon \tag{7.4}$$

where l is the model length. However for the purpose of this simulations we will use the former method.

Visualization software OVITO was used to view snapshots of the simulation. As can be observed in figure 7.1, folds appear in the graphene sheet under tension, which is typical in a pre-cracked graphene sheet under stress.

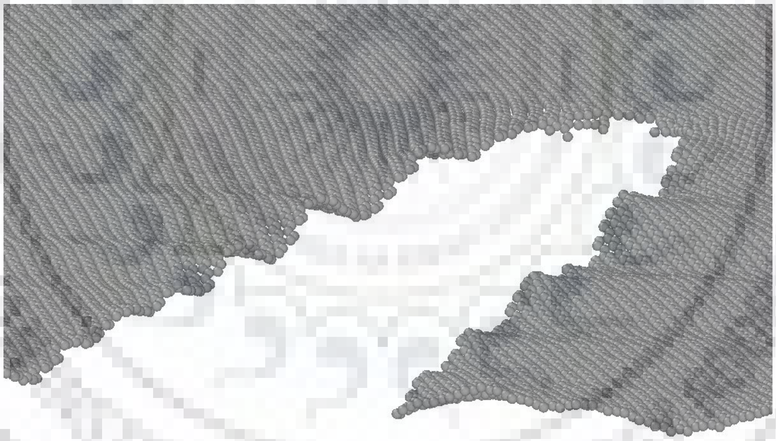

FIGURE 7.1: Folds appear on the graphene sheet under strain

Figure 7.2 show the snapshots at different time steps of graphene sheet under strain fracture in a strain controlled loading. The model was loaded for about 0.038 ns until the first void appeared behind the crack front. These voids are nucleation points at which stress concentrates and the crack propagates through [14]. As can be seen from the zoomed snapshot 7.3 with virial stress y direction component per atom, the stress is higher than its surrounding near the void region. After the void appeared and crack stated the fracture occurred suddenly in about 0.0025 ns.

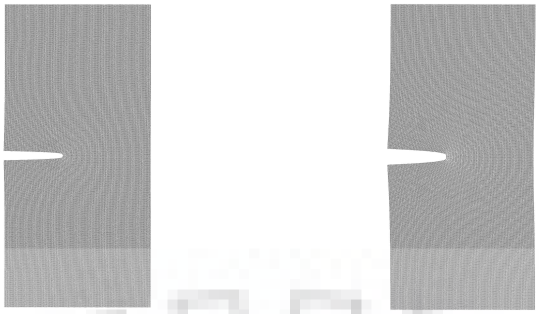

(A) Crack at 0.015 ns (B) Crack at 0.0383 ns

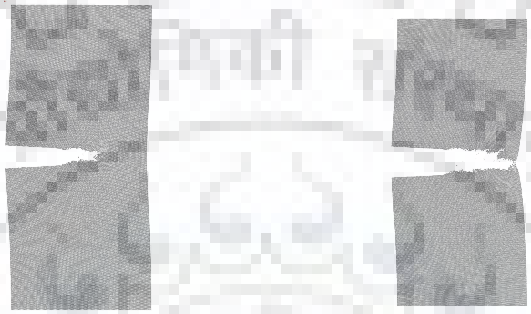

(C) Crack at 0.04 ns (D) Crack at 0.0408 ns

FIGURE 7.2: Snapshots of SLGS undergoing fracture at different time-steps

The stress-strain graph 7.4 obtained through fracture simulation show a typical brittle fracture behavior. The rupture strength obtained by this method was around observed to 21.78 GPa which is very close to 21.1 GPa reported by P. Zhang et al[46] while the strain at which the fracture occurs was also very close at 0.0383 vs 0.026 obtained by them.

From the fracture strength, we can now calculate the surface energy as well as the critical energy release rate. Rearranging 7.3 and putting the σ_f equal to 21.78 GPa ,a as 10nm, E equal to 888.88 GPa as obtained in previous simulations and α as 1.12, we obtain the critical energy release G_c as 20.8 jm^{-2}. In the literature the values for G_c is given any wherefrom 10.4 jm^{-2} [17] to 15.9 jm^{-2} [44] which varies with the result obtained . However, the difference is small and can be neglected for the purpose of this thesis.

7.3 Phase Field Modeling

The values obtained and verified through molecular dynamics are will now be used to model the phase field model as discussed in chapter 4 for the graphene sheet. The phase field graphene sheet will be of the same dimension 20nm x 10nm as the molecular dynamics sheet to corroborate results.

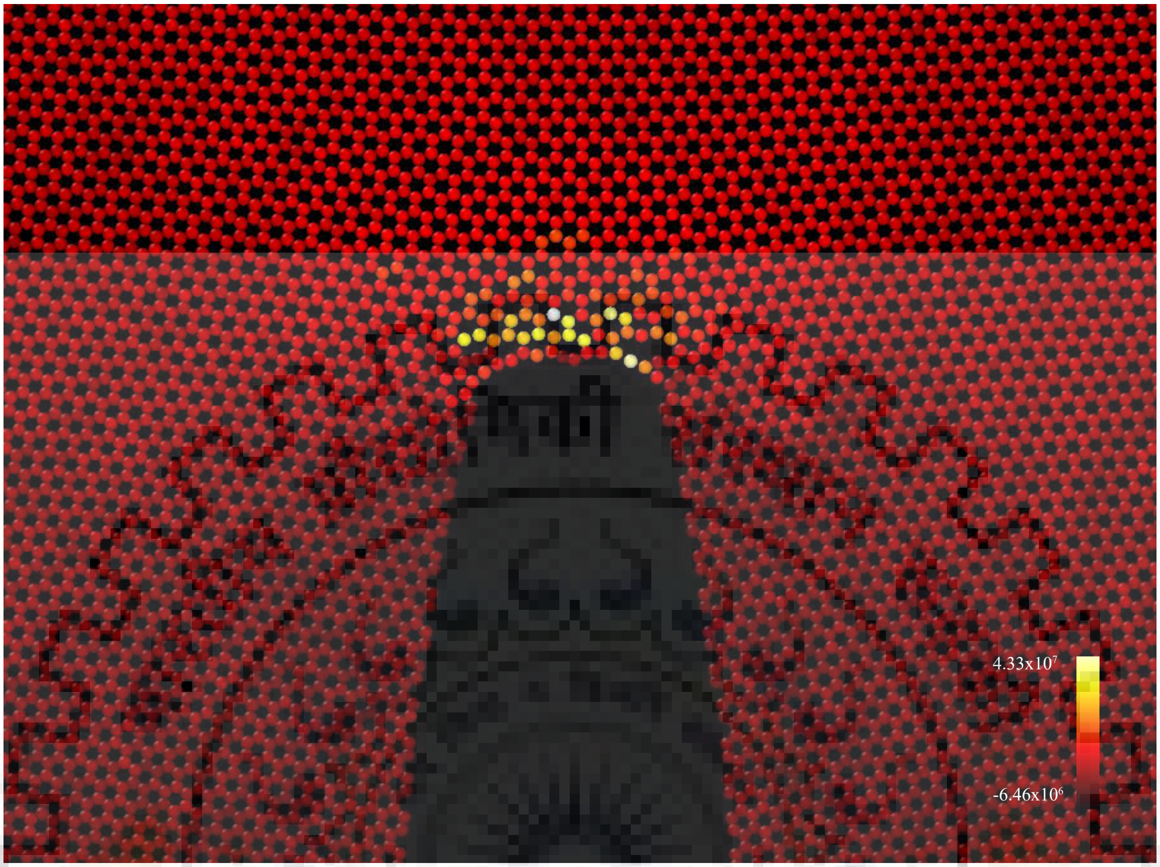
4.33x10^7
-6.46x10^6

FIGURE 7.3: Stress concentration near the crack

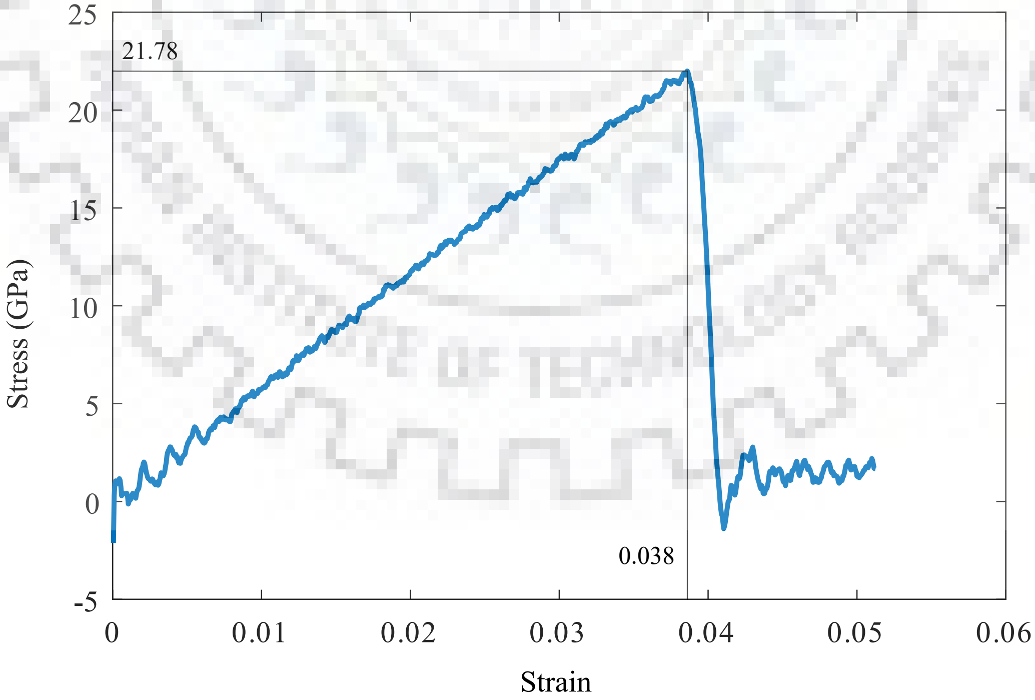

FIGURE 7.4: Stress-strain curve of graphene sheet

The codes for phase field modeling were written in MATLAB owing to its vector and matrix function library. A finite element mesh was generated from a freely available mesh generation code consisting of 4141 nodes which make up 4000 elements. These elements were 4 node isoparametric elements. The crack was introduced manually through a crack array. Mesh was refined in the area of the expected crack path. Similar to molecular dynamics simulation the load is applied in a displacement controlled manner in which the displacement was applied at nodes at the top edge with an increment of 0.0035 nm per time step.

The parameters to be used for the phase field simulation are stated below

$G_c(j/m^{-2})$	E(GPa)	ν	$l_0(nm)$	k	η(GPa)
20.8	888.88	0.234	0.125	1.0x10^{-6}	2x888.88

As shown in figure 7.6 the phase field crack model can be seen evolving in time under constant strain rate. The phase field parameter ϕ which here represents the cracked or intact region can be observed as being regions where the value of ϕ is 1 and 0 respectively. At the 0_{th} time step 7.6a the pre-cracked phase field model can be seen which is similar to the molecular dynamics model in all dimensions. However, in this model, the plate is considered truly 2-D therefore the question of stress is out of the question. Therefore it is much more convenient and resource efficient to obtain a force-displacement graph in this case.

As the strain increases the strain energy accumulates near the crack tip. It takes some time before the strain energy becomes equal to the critical energy release rate G_c when the crack propagation happens. This is in accordance with Griffith's criterion as discussed in 3.2.1. As can be seen from figure 7.6b the stress concentration changes the crack morphology

At time step 2075 7.6c the strain energy becomes greater than critical energy release rate and the energy is released in the form of crack propagation. The crack is sudden until it branches at time step 2350 7.6d which also decreases crack velocity just before the sheet fractures completely.

The force-displacement graph showing brittle behavior is shown in figure 7.5. The graph shows a typical load-displacement behavior of brittle material. The curve peaks at 76.16 nanonewton corresponding to the displacement of 0.4746 nanometres. The transition zone between the cracked and intact surface can be observed.

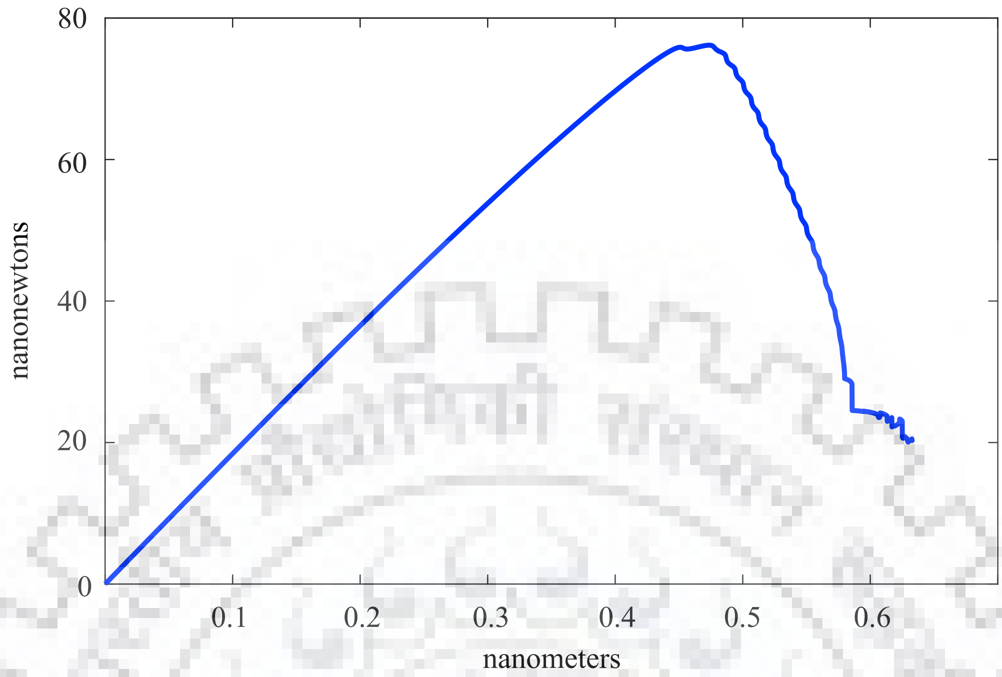

FIGURE 7.5: Load-displacement graph of phase field model

7.4 Discussion

The results of the two different modelings and simulation technique of the materials of the same dimensions and crack length results varies from being very agreeable to being significantly different. The crack path predicted by both the simulation techniques is in agreement with each other. The point at which the crack branching occurs is also very similar. Crack path and branching prediction is an important part of the variation formulation of fracture criterion of which phase field model is a regularized version of.

The force-displacement also appears to show similarity in terms of the load at which the fracture occurs. The phase field fracture force was calculated to be 76.16 nanonewton while molecular dynamics fracture was calculated to be 72.92 nanonewton. This can be regarded as nearly identical results. The error between the two fracture force can be calculated as

$$error(\%) = \frac{76.16 - 72.92}{72.92} = 0.044 \tag{7.5}$$

which is equal to 4.4 percent.

However few differences also arise between the phase field and molecular dynamics simulations results. As can be seen in the combined force-displacement graphs of the two

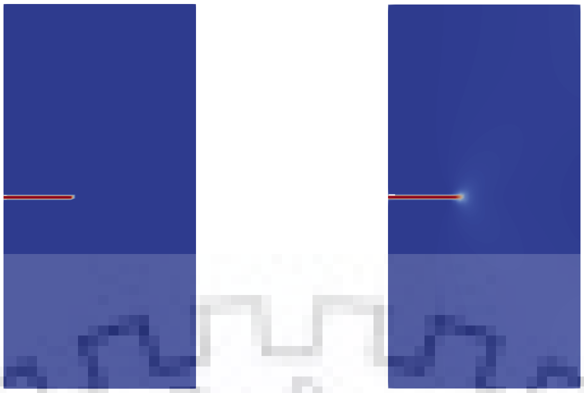

(A) Crack at 0 time-step (B) Crack at 1975 time-step

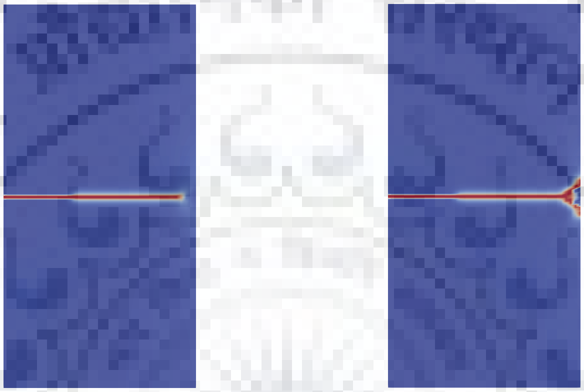

(C) Crack at 2075 time-step (D) Crack at 2350 time-step

FIGURE 7.6: Snapshots phase field model undergoing fracture at different time-steps

simulations the displacement at which the fracture occurs is different. Although in absolute term the difference is not much, in relative terms the difference is significant. The fracture strain for phase field model is 0.4736 nm while in the molecular dynamics model it was 0.78297 nm. From the data given above we can calculate the simplified stiffness predicted by the two models as

$$Stiffness = \frac{Force}{Displacement} \tag{7.6}$$

for molecular dynamics model the stiffness was calculated as 93.13255 nm^{-1} while, phase field model's stiffness was calculated being equal to 160.81nm^{-1}. the percentage error between the two being 72.7 percent.

The discrepancy between the results may be due to the face that MD simulation allows for model deformation in the form of body translation and rotation which is not the case

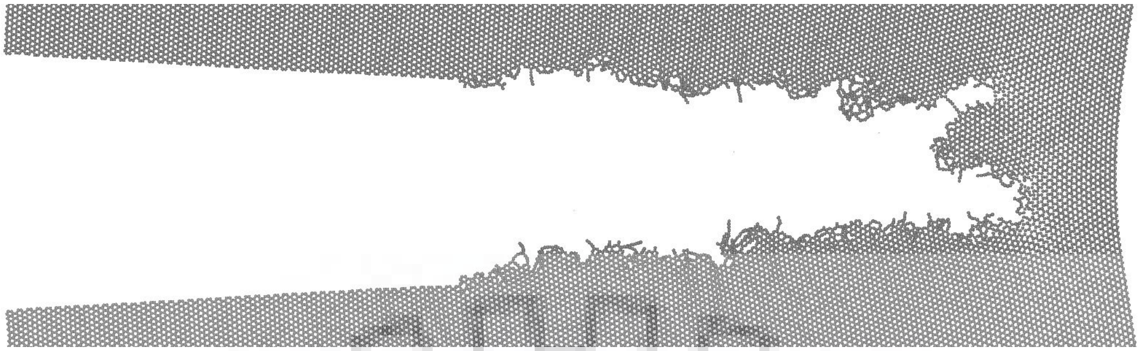

(A) MD crack branching

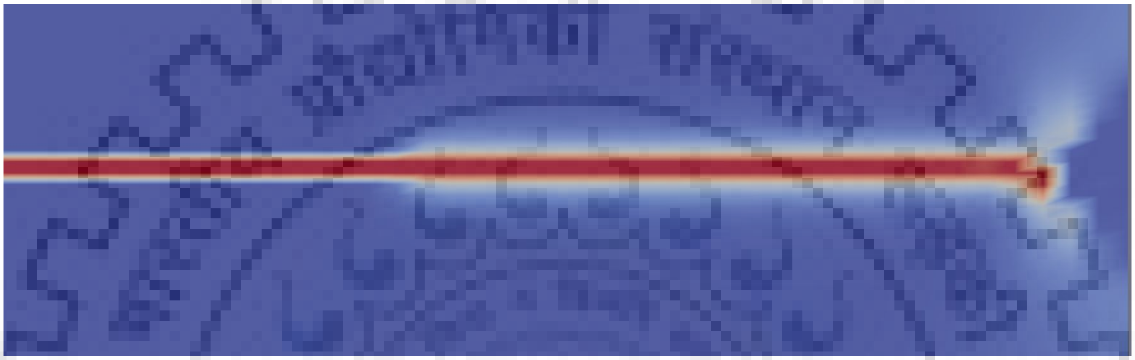

(B) PF crack branching

FIGURE 7.7: Similarity between the crack branching prediction between MD and PFM

with phase field model. In the continuum model, this is constrained by fixing vertical displacement between two nodes. As a result of this fixing, it may cause the model to have asymmetry despite deformation causing it to appear artificially stiffened, which may then cause of the difference in the displacement results given that displacement of phase field model is relatively small.

Another reason for the differences in results could be due to the fact that graphene has a strain-dependent elastic modulus. Atomic simulations can capture this non-linear behavior very naturally while this is not the case with the phase field model. It is possible to create a phase field model in which the elastic modulus can be modeled as a function of strain eliminating or confirming this as the source of error.

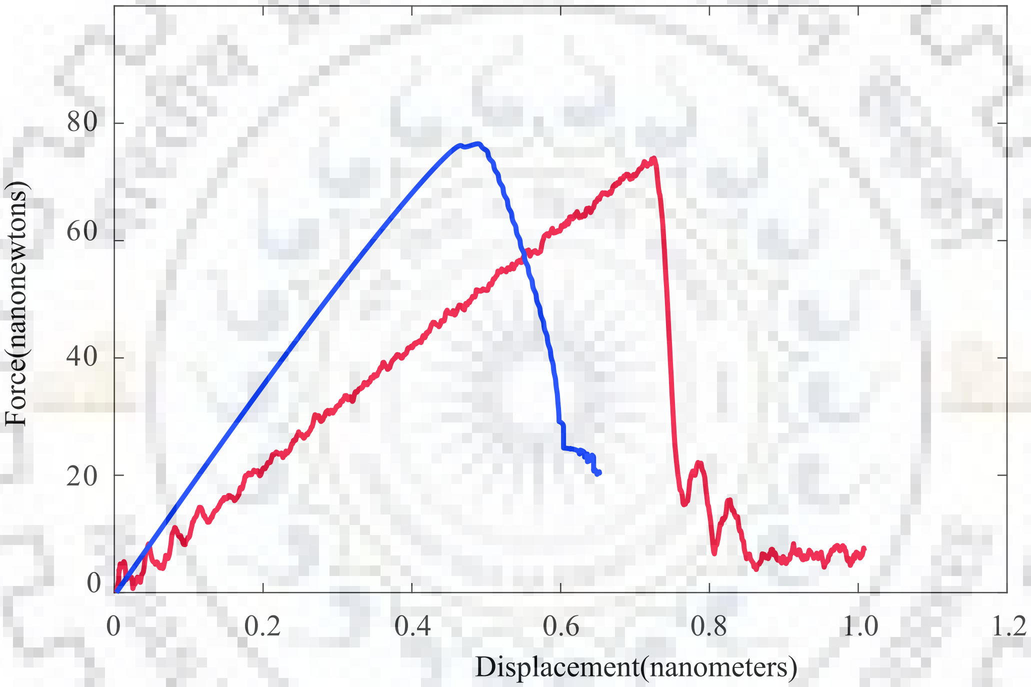

FIGURE 7.8: Combined load-displacement graphs of MD and PF models.

Chapter 8

Conclusion and future prospects

8.1 Conclusion

Continuum mechanics can tackle a variety of problems pertaining to the engineering aspect of problem-solving. Different levels of simplifications are applied to the problems which cannot be solved by molecular dynamics in a practical way. Molecular dynamics, on the other hand, goes deeper into the details and have much fewer simplifications, however for finite resources there is a trade-off between scale and details of the simulation. Despite these conceptual differences between the two modeling schemes concept of combining the two simulations is promising. The parameters required for the continuum model can be obtained from physics based molecular dynamics modeling making the overall approach closer to physics and reducing the dependence of empiricism. The efficiency of continuum mechanics allows for the inference of the properties at the molecular scale to be implemented at bigger scales helping us understand the dependence of atomic scale properties on its macro properties.

Continuum models are generally less resource intensive compared to atomistic models. In my testing atomic simulation tool 3 to 4 times longer to be performed despite using 4 CPU-cores compared to 1 for phase field model. Thus a combined continuum and atomistic approach can also help draw conclusions faster retaining atomistic information.

In this study atomic description of fracture of graphene sheet under uniaxial tension at the nanoscale is provided. The mechanical properties obtained through it are in good agreement with previous literature on both molecular dynamics simulation and experimental studies. The ability of phase field model to describe a fracture with the help of MD properties was confirmed. Obtaining key parameters from MD simulation, it shows convergence between the results in two key areas as reported in the literature. Key conclusions are stated below.

- Continuum phase field model can be used to study fracture problems with properties obtained from molecular dynamics.
- The phase field model could predict the path of the crack along with crack branching under uniaxial tensile stress. This is the main component of the regulrized version of variational approach for fracture.
- Force at which the material fractures were similar for both the modeling techniques and were within 4.4% of each other.
- Stiffness calculated from the force displacement graphs show significant variation of 72 % between the two simulation techniques. The possible reason for this has been discussed in chapter 7.

8.2 Future work

In this study, some deviation between the results was also noted, along with probable causes of its occurrence. As this is a novel approach much work and studies remain to be done in improving the existing results and also in furthering the scope of this mode of modeling.

For improving the existing results to better match the results obtained through atomistic simulation of material which have a nonlinear response to strain implementation of strain-dependent phase field model is to be on the lookout. Fracture model which incorporate other modes of fracture under different setups (shear, different geometry, etc.) is to be modeled.

Phase field modeling has been used to study qualitatively a variety of time evolution problem outside the scope of mechanics. For example, PF has been used in the study of phase transformation and fluid dynamics. Phase field models in these domains can also be developed which obtains relevant parameters through atomistic simulations.

Bibliography

[1] S. M. Allen and J. W. Cahn. “Ground state structures in ordered binary alloys with second neighbor interactions”. In: *Acta Metallurgica* 20.3 (1972), pp. 423–433. DOI: 10.1016/0001-6160(72)90037-5.

[2] Marreddy Ambati, Tymofiy Gerasimov, and Laura Lorenzis. “A Review on Phase-field Models of Brittle Fracture and a New Fast Hybrid Formulation”. In: *Comput. Mech.* 55.2 (Feb. 2015), pp. 383–405. DOI: 10.1007/s00466-014-1109-y.

[3] Luigi Ambrosio and Vincenzo Maria Tortorelli. “Approximation of functional depending on jumps by elliptic functional via t-convergence”. In: *Communications on Pure and Applied Mathematics* 43.8 (1990), pp. 999–1036. DOI: 10.1002/cpa.3160430805.

[4] Hanen Amor, Jean Jacques Marigo, and Corrado Maurini. “Regularized formulation of the variational brittle fracture with unilateral contact: Numerical experiments”. In: *Journal of the Mechanics and Physics of Solids* 57.8 (2009), pp. 1209–1229. DOI: 10.1016/j.jmps.2009.04.011.

[5] Tsuneya Ando. “The electronic properties of graphene and carbon nanotubes”. In: *NPG Asia Materials* 1.1 (2009), pp. 17–21. DOI: 10.1038/asiamat.2009.1.

[6] Emilio Artacho et al. “Sánchez-Portal_Phys._Rev._B_1999.pdf VN - readcube.com”. In: *Physical Review B* 59.19 (1999), pp. 12678–12688.

[7] T. Belytschko et al. “Atomistic simulations of nanotube fracture”. In: *Physical Review B - Condensed Matter and Materials Physics* 65.23 (2002), pp. 2354301–2354308. DOI: 10.1103/PhysRevB.65.235430.

[8] Andrea L. Bertozzi, Selim Esedoglu, and Alan Gillette. “Inpainting of binary images using the Cahn-Hilliard equation”. In: *IEEE Transactions on Image Processing* 16.1 (2007), pp. 285–291. DOI: 10.1109/TIP.2006.887728.

[9] B. Bourdin, G. A. Francfort, and J. J. Marigo. “Numerical experiments in revisited brittle fracture”. In: *Journal of the Mechanics and Physics of Solids* 48.4 (2000), pp. 797–826. DOI: 10.1016/S0022-5096(99)00028-9.

[10] Blaise Bourdin, Gilles A. Francfort, and Jean Jacques Marigo. *The variational approach to fracture*. 2008, pp. 1–164. DOI: 10.1007/978-1-4020-6395-4.

[11] Blaise Bourdin et al. *The variational approach to fracture To cite this version : The variational approach to fracture*. Vol. 91. 2011, pp. 5–148.

[12] Emiliano Cadelano et al. “Nonlinear elasticity of monolayer graphene”. In: *Physical Review Letters* 102.23 (2009), pp. 1–4. DOI: 10.1103/PhysRevLett.102.235502.

[13] John W. Cahn and John E. Hilliard. “Free energy of a nonuniform system. I. Interfacial free energy”. In: *The Journal of Chemical Physics* 28.2 (1958), pp. 258–267. DOI: 10.1063/1.1744102.

[14] S. Chandra et al. “Molecular dynamics simulations of crack growth behavior in Al in the presence of vacancies”. In: *Computational Materials Science* 117 (2016), pp. 518–526. DOI: 10.1016/j.commatsci.2016.02.032.

[15] T. Chang and H. Gao. “Size-dependent elastic properties of a single-walled carbon nanotube via a molecular mechanics model”. In: *Journal of Mechanics Physics of Solids* 51 (June 2003), pp. 1059–1074. DOI: 10.1016/S0022-5096(03)00006-1.

[16] Vittorio Cristini et al. “Nonlinear simulations of solid tumor growth using a mixture model: Invasion and branching”. In: *Journal of Mathematical Biology* 58.4-5 (2009), pp. 723–763. DOI: 10.1007/s00285-008-0215-x.

[17] M. A.N. Dewapriya, R. K.N.D. Rajapakse, and A. S. Phani. “Atomistic and continuum modelling of temperature-dependent fracture of graphene”. In: *International Journal of Fracture* 187.2 (2014), pp. 199–212. DOI: 10.1007/s10704-014-9931-y.

[18] CHARLES M ELLIOTT and DONALD A FRENCH. “Numerical Studies of the Cahn-Hilliard Equation for Phase Separation”. In: *IMA Journal of Applied Mathematics* 38.2 (1987), pp. 97–128. DOI: 10.1093/imamat/38.2.97.

[19] G. A. Francfort and J.-J. Marigo. “Revisiting brittle fracture as an energy minimization problem”. In: *Journal of Mechanics Physics of Solids* 46 (Aug. 1998), pp. 1319–1342. DOI: 10.1016/S0022-5096(98)00034-9.

[20] H Garcke et al. "A continuous Clustering Method for vector fields". In: *Visualization 2000* (2000), pp. 351–358. DOI: `10.1109/VISUAL.2000.885715`.

[21] Shuchi Gupta, K. Dharamvir, and V. K. Jindal. "Elastic moduli of single-walled carbon nanotubes and their ropes". In: *Physical Review B - Condensed Matter and Materials Physics* 72.16 (2005), pp. 1–16. DOI: `10.1103/PhysRevB.72.165428`.

[22] Y. Jin and F. G. Yuan. "Atomistic Simulations of J-Integral in 2D Graphene Nanosystems". In: *Journal of Nanoscience and Nanotechnology* 5.12 (2005), pp. 2099–2107. DOI: `doi:10.1166/jnn.2005.414`.

[23] Yuhang Jing et al. "Chirality and Size Dependent Elastic Properties of Silicene Nanoribbons under Uniaxial Tension". In: *Beijing Conference* Md (2013), pp. 1–6.

[24] Rajiv K. Kalia et al. "Role of Ultrafine Microstructures in Dynamic Fracture in Nanophase Silicon Nitride". In: *Phys. Rev. Lett.* 78 (11 Mar. 1997), pp. 2144–2147. DOI: `10.1103/PhysRevLett.78.2144`.

[25] Hideaki Kikuchi et al. "Brittle dynamic fracture of crystalline cubic silicon carbide (3C-SiC) via molecular dynamics simulation". In: *Journal of Applied Physics* 98.10 (2005). DOI: `10.1063/1.2135896`.

[26] Junseok Kim. "A continuous surface tension force formulation for diffuse-interface models". In: *Journal of Computational Physics* 204.2 (2005), pp. 784–804. DOI: `10.1016/j.jcp.2004.10.032`.

[27] Konstantin N. Kudin, Gustavo E. Scuseria, and Boris I. Yakobson. "(formula presented) BN, and C nanoshell elasticity from ab initio computations". In: *Physical Review B - Condensed Matter and Materials Physics* 64.23 (2001), pp. 1–10. DOI: `10.1103/PhysRevB.64.235406`.

[28] Charlotte Kuhn, Alexander Schlüter, and Ralf Müller. "A Phase Field Approach for Dynamic Fracture". In: *Pamm* 13.1 (2013), pp. 87–88. DOI: `10.1002/pamm.201310039`.

[29] Christopher J. Larsen. "Models for dynamic fracture based on Griffith's criterion". In: *IUTAM Bookseries* 21 (2010), pp. 131–140. DOI: `10.1007/978-90-481-9195-6-10`.

[30] Minh Quy Le and Romesh C. Batra. “Single-edge crack growth in graphene sheets under tension”. In: *Computational Materials Science* 69 (2013), pp. 381–388. DOI: 10.1016/j.commatsci.2012.11.057.

[31] Fang Liu, Pingbing Ming, and Ju Li. “Ab initio calculation of ideal strength and phonon instability of graphene under tension”. In: *Physical Review B - Condensed Matter and Materials Physics* 76.6 (2007), pp. 1–7. DOI: 10.1103/PhysRevB.76.064120.

[32] QIANG LU and RUI HUANG. “Nonlinear Mechanics of Single-Atomic-Layer Graphene Sheets”. In: *International Journal of Applied Mechanics* 01.03 (2009), pp. 443–467. DOI: 10.1142/s1758825109000228.

[33] Christian Miehe, Martina Hofacker, and Fabian Welschinger. “A phase field model for rate-independent crack propagation: Robust algorithmic implementation based on operator splits”. In: *Computer Methods in Applied Mechanics and Engineering* 199.45-48 (2010), pp. 2765–2778. DOI: 10.1016/j.cma.2010.04.011.

[34] David Mumford and Jayant Shah. “Optimal approximations by piecewise smooth functions and associated variational problems”. In: *Communications on Pure and Applied Mathematics* 42.5 (1989), pp. 577–685. DOI: 10.1002/cpa.3160420503.

[35] Andrey Omeltchenko et al. “Crack front propagation and fracture in a graphite sheet: A molecular-dynamics study on parallel computers”. In: *Physical Review Letters* 78.11 (1997), pp. 2148–2151. DOI: 10.1103/PhysRevLett.78.2148.

[36] Qing-Xiang Pei, Yong-Wei Zhang, and Vivek B Shenoy. “Mechanical properties of methyl functionalized graphene: a molecular dynamics study.” In: *Nanotechnology* 21.11 (2010), p. 115709. DOI: 10.1088/0957-4484/21/11/115709.

[37] Rassin Grantab, Vivek B. Shenoy, and Rodney S. Ruoff. “Anomalous stregth characterictics of tilt grain boundaries in graphene”. In: *Science* 330.November (2010), p. 946.

[38] C D Reddy, S Rajendran, and K M Liew. “Equilibrium configuration and continuum elastic properties of finite sized graphene”. In: *Nanotechnology* 17.3 (Jan. 2006), pp. 864–870. DOI: 10.1088/0957-4484/17/3/042.

[39] C. L. Rountree et al. “A unified study of crack propagation in amorphous silica: Using experiments and simulations”. In: *Journal of Alloys and Compounds* 434-435.SPEC. ISS. (2007), pp. 60–63. DOI: `10.1016/j.jallcom.2006.08.336`.

[40] Cindy L. Rountree et al. “Atomistic Aspects of Crack Propagation in Brittle Materials: Multimillion Atom Molecular Dynamics Simulations”. In: *Annual Review of Materials Research* 32.1 (2002), pp. 377–400. DOI: `10.1146/annurev.matsci.32.111201.142017`.

[41] Steven J Stuart et al. “A second-generation reactive empirical bond order (REBO) potential energy expression for hydrocarbons”. In: *Journal of Physics: Condensed Matter* 14.4 (2002), pp. 783–802. DOI: `10.1088/0953-8984/14/4/312`.

[42] Clemens V. Verhoosel and René de Borst. “A phase-field model for cohesive fracture”. In: *International Journal for Numerical Methods in Engineering* 96.1 (2013), pp. 43–62. DOI: `10.1002/nme.4553`.

[43] Xiaoding Wei et al. “Nonlinear elastic behavior of graphene: Ab initio calculations to continuum description”. In: *Physical Review B - Condensed Matter and Materials Physics* 80.20 (2009), pp. 1–8. DOI: `10.1103/PhysRevB.80.205407`.

[44] Hanqing Yin et al. “Griffith criterion for brittle fracture in graphene”. In: *Nano Letters* 15.3 (2015), pp. 1918–1924. DOI: `10.1021/nl5047686`.

[45] Liangzhe Zhang et al. “Phase-field modeling of temperature gradient driven pore migration coupling with thermal conduction”. English (US). In: *Computational Materials Science* 56 (Apr. 2012), pp. 161–165. DOI: `10.1016/j.commatsci.2012.01.002`.

[46] Peng Zhang et al. “Fracture toughness of graphene”. In: *Nature Communications* 5 (2014), pp. 1–7. DOI: `10.1038/ncomms4782`.